Genetic insights into biological mechanisms governing human ovarian ageing

Ruth, K.S.; Day, F.R.; Hussain, J.; Martinez-Marchal, A.; Aiken, C.E.; Azad, A.; ... ; 23 Me Res Team

Article

Genetic insights into biological mechanisms governing human ovarian ageing

https://doi.org/10.1038/s41586-021-03779-7

Received: 24 August 2020

Accepted: 29 June 2021

Published online: 4 August 2021

Check for updates

Reproductive longevity is essential for fertility and influences healthy ageing in women[1,2], but insights into its underlying biological mechanisms and treatments to preserve it are limited. Here we identify 290 genetic determinants of ovarian ageing, assessed using normal variation in age at natural menopause in approximately 200,000 women of European ancestry. These common alleles were associated with clinical extremes of age at natural menopause; women in the top 1% of genetic susceptibility have an equivalent risk of premature ovarian insufficiency to those carrying monogenic *FMR1* premutations[3]. The identified loci implicate a broad range of DNA damage response (DDR) processes and include loss-of-function variants in key DDR-associated genes. Integration with experimental models demonstrates that these DDR processes act across the life-course to shape the ovarian reserve and its rate of depletion. Furthermore, we demonstrate that experimental manipulation of DDR pathways highlighted by human genetics increases fertility and extends reproductive life in mice. Causal inference analyses using the identified genetic variants indicate that extending reproductive life in women improves bone health and reduces risk of type 2 diabetes, but increases the risk of hormone-sensitive cancers. These findings provide insight into the mechanisms that govern ovarian ageing, when they act, and how they might be targeted by therapeutic approaches to extend fertility and prevent disease.

Over the past 150 years, life expectancy in developed countries has increased from 45 to 85 years[4], but the timing of reproductive senescence (age at natural menopause (ANM)) has remained relatively constant (50–52 years)[5]. The genetic integrity of oocytes decreases with advancing age[6] and natural fertility ceases about 10 years before menopause[1]. More women are choosing to delay childbearing to older ages, resulting in increased use of assisted conception techniques[7,8]. Preservation of oocytes and ovarian tissue can prolong fertility, but it is invasive and there is only an approximately 6.5% chance of achieving pregnancy with each mature oocyte thawed, which decreases with age[9].

ANM is determined by the non-renewable ovarian reserve, which is established during fetal development and continuously depleted until reproductive senescence (Extended Data Fig. 1). The DNA damage response (DDR) is the primary biological pathway that regulates reproductive senescence, as highlighted by genome-wide association studies (GWAS)[10], rare single-gene disorders that cause premature ovarian insufficiency (POI)[11] and animal models[12]. A better understanding of how and when molecular processes influence the establishment and decline of the ovarian reserve will inform future strategies for treating infertility and preserving fertility. Our results increase the number of known ANM-associated genetic loci fivefold[13], from 56 to 290. We integrate these data with experiments in mice to characterize the specific DDR processes that contribute to reproductive ageing, providing insights into when they act across the life-course, how they might be modified to preserve fertility and the potential consequences for broader health.

Results

Genome-wide array data, imputed to approximately 13.1 million genetic variants with minor allele frequency (MAF) ≥ 0.1%, were available for 201,323 women of European ancestry (Extended Data Fig. 2, Supplementary Table 1). We identified 290 statistically independent signals associated with ANM ($P < 5 \times 10^{-8}$), including six on the X chromosome, which has, to our knowledge, not previously been tested in large-scale studies (Fig. 1, Supplementary Table 2). Effect estimates for the 290 signals were consistent between linear and Cox proportional hazard models and across strata of the meta-analysis (Extended Data Fig. 3). There was no evidence of test statistic inflation due to population structure (linkage disequilibrium (LD) score intercept 1.02, s.e. 0.03). All previously reported signals[13] retained genome-wide significance (Fig. 1).

Additive, per-allele effect sizes for the 290 signals ranged from about 3.5 weeks to about 74 weeks (Fig. 1, Extended Data Fig. 2, Supplementary Table 2). Three of these variants exhibited non-additive effects (Extended Data Fig. 4a–d, Supplementary Table 3, Supplementary Results). We sought to replicate our 290 signals using independent samples from 23andMe (n = 294,828 women). We observed high concordance in effect estimates between the datasets (Supplementary Table 2, Extended Data Fig. 3g), with nearly all variants at least nominally associated with ANM in the 23andMe data. Eight variants fell below genome-wide significance in a meta-analysis of our discovery with 23andMe ($P_{max} = 2.6 \times 10^{-5}$), half the number of expected false-positive associations ($290 \times 0.05 = 14.5$). We next evaluated these loci in 78,317 women of East Asian ancestry. There was broad replication, consistent

A list of authors and their affiliations appears online. ✉e-mail: eva@sund.ku.dk; a.murray@exeter.ac.uk; ignasi.roig@uab.cat; john.perry@mrc-epid.cam.ac.uk

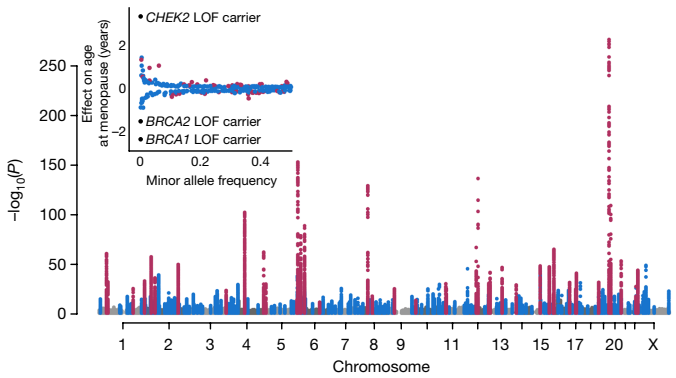

Fig. 1 | Manhattan plot representing GWAS discovery analysis. Purple, previously identified loci; blue, newly identified loci. Plotted variants have $P < 0.01$ with $P < 1 \times 10^{-300}$ truncated. Inset, effect sizes and MAFs of the loci.

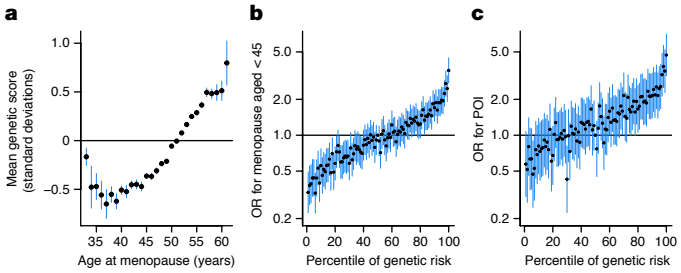

Fig. 2 | Polygenic prediction of age at menopause. a, Mean PGS (scaled to have mean = 0, s.d. = 1) for a given ANM. Higher PGS indicates later ANM. **b**, **c**, Association of each centile of PGS compared with the 50th centile with early menopause (**b**) and premature ovarian insufficiency (**c**). Error bars indicate 95% CI.

with previous observations[14], but substantial heterogeneity of effect sizes and allele frequencies (Supplementary Table 2). This was exemplified at the *ENTPD1* locus, where one signal had an effect size around three times larger in the East Asian cohort than in the European cohort (rs1889921), whereas a second independent signal about 20 kb away had an effect estimate half the size in the East Asian group (rs7087644).

Using additional independent samples from the deCODE study ($n = 16{,}556$ women), we estimated that our identified signals cumulatively explained 10.1% of the variance in ANM. This compared to an estimate of 12.3% in the UK Biobank (UKBB) using weights for the 290 variants derived from our non-UKBB samples (Supplementary Table 2). The identified signals therefore account for 31–38% of the overall genotype-array estimated heritability in UKBB ($h^2_g = 32.4\%$, s.e. 0.8%), compared to 15.7–19.8% for the 56 previously reported signals (Extended Data Fig. 4e).

Common variants act on extremes of ANM

It is unclear where in the population distribution of ANM the influence of common genetic variants begins and ends. Our GWAS was restricted to the 99% of women with ANM between 40 and 60 years of age. ANM before 40 years (POI) is considered a Mendelian disorder, but may have a polygenic component. To test which parts of the ANM distribution are influenced by common genetic variation, we calculated a polygenic score (PGS) for 108,840 women in the UKBB with the full range of ANM using genetic weights derived from the independent non-UKBB component of the meta-analysis (Supplementary Table 2). This was coded such that a higher PGS indicates increased susceptibility to later ANM. ANM from 34 to 61 years had a significant polygenic influence (Fig. 2a). For example, women with ANM at 34 years had a PGS that was on average −0.5 s.d. (95% confidence interval (CI) 0.26–0.69, $P = 1.5 \times 10^{-5}$) lower than the population mean. We had limited sample size to test outside these age ranges, but there was some evidence for depletion of polygenic influence at ages below 34 years (Fig. 2a). These data suggest that common genetic variants act on clinically relevant extremes of ANM, although it remains unclear what fraction of POI cases might be polygenic as opposed to monogenic.

We also evaluated the predictive ability of the PGS. Genetic risk alone proved to be a weak predictor (receiver operating characteristics area under the curve (ROC-AUC) 0.65 and 0.64 for early menopause (age <45 years) and POI, respectively) (Fig. 2b, c), but the PGS performed substantially better than smoking status, which is the most robust epidemiologically associated risk factor (ROC-AUC 0.58). Adding smoking status to the PGS did not appreciably improve the prediction of early menopause (ROC-AUC 0.66). Despite its low overall discriminative ability, the PGS was able to identify individuals at high risk of POI (Fig. 2c). Women in the top 1% of PGS (rescaled such that high PGS indicates increased susceptibility to earlier menopause) had equivalent POI risk (PGS odds ratio (OR) 4.71 (95% CI 3.15–7.04) versus 50th centile, $P = 4.4 \times 10^{-14}$) to that reported for women with premutations in *FMR1*, the leading tested monogenic cause of POI (OR ≈ 5)[3]. It is, however, notable that the top 1% of genetic risk is more prevalent than the *FMR1* premutation carrier rate (1:250).

Functional genes and pathways implicated

We used a combination of in silico fine mapping and expression quantitative trait loci (eQTL) data to identify putatively functional genes implicated by our genetic association signals (Supplementary Table 2). First, 81 of the 290 independent ANM signals were highly correlated (minimum $r^2 = 0.8$) with one or more variants that were predicted to be deleterious for gene function, implicating 91 genes (Supplementary Table 4). Twelve of these genes contained predicted loss-of-function (LOF) variants, and seven genes (*MCM8*, *EXO1*, *HELB*, *C1orf112*, *C19orf57*, *FANCM* and *FANCA*) contained multiple statistically independent predicted-deleterious variants (Supplementary Table 4). We extended this analysis using exome sequence data from 45,351 women in the UKBB. LOF variants near two highlighted genes were associated with ANM (Supplementary Table 5). In aggregate, women carrying LOF variants in *BRCA2* ($n = 143$) and *CHEK2* ($n = 68$) reported ANM 1.54 years earlier (95% CI 0.73–2.34, $P = 6.8 \times 10^{-5}$) and 3.49 years later (95% CI 2.36–4.63, $P = 1 \times 10^{-13}$), respectively, than non-carriers. *BRCA1* LOF was the next most significantly associated GWAS-highlighted gene in these analyses ($n = 32$ LOF carriers, 2.63 years earlier ANM, 95% CI 1.00–4.26, $P = 1.1 \times 10^{-4}$). Homozygous LOF variants in *BRCA2* were recently described as a rare cause of POI[15], but we did not identify any such homozygotes for *BRCA2*, *CHEK2* or *BRCA1*. Notably, identified GWAS signals mapped within 300 kb of 20 out of 74 genes that, when disrupted, cause primary amenorrhea and/or POI (Supplementary Table 6), highlighting that normal variation in reproductive ageing and clinical extremes share common biological processes.

Next, we integrated publicly available data for gene expression across 44 tissue types with our GWAS results (Supplementary Table 5). This highlighted expression-linked genes at 116 of the 290 loci (Supplementary Tables 2, 5). Using three computational approaches, we observed enrichment of ANM-associated variants in genes expressed in haematopoietic stem cells and their progenitors (Supplementary Tables 7–12). Biological pathway enrichment analyses, using a range of approaches, highlighted the importance of DDR processes as the key regulator of ANM (Supplementary Tables 13–16). We hypothesize that the shared expression profile in both haematopoietic stem cells and oocytes reflects the relative importance of DDR in both cell types[16]. Unlike the timing of puberty[17], which represents the beginning of reproductive life, the timing of ANM was not associated with enrichment

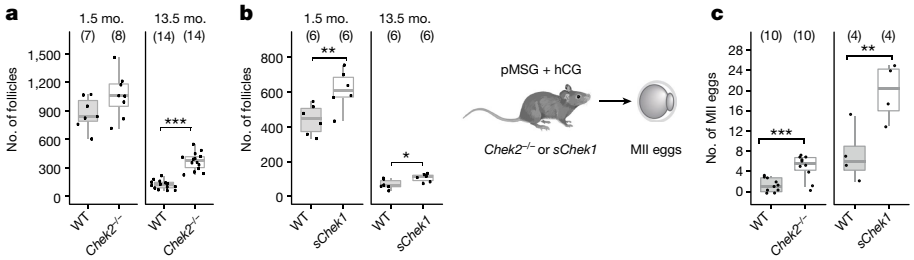

Fig. 3 | Genetic manipulation of *Chek1* or *Chek2* extends reproductive lifespan in mice. a, **b**, Numbers of follicles in young and aged *Chek2*$^{-/-}$ (**a**) and *sChek1* (**b**) female mice. Numbers of ovaries analysed in parentheses. **c**, Response to gonadotrophin stimulation of 13.5-month-old *Chek2*$^{-/-}$ and 11- to 13-month-old *sChek1* females assessed by the number of MII oocytes retrieved. Numbers of stimulated females in parentheses. For box plots, centre line, median; box limits, interquartile range (IQR); whiskers, 1.5 × IQR. hCG, human chorionic gonadotrophin; pMSG, pregnant mare serum gonadotrophin. Two-sample *t*-test; **P* < 0.05, ***P* < 0.025, ****P* < 0.001.

of genes expressed in the hypothalamus and pituitary gland, but was associated with enrichment of genes expressed in the ovary and other reproductive tissues (Supplementary Table 9).

Finally, we attempted to leverage data from multi-tissue co-expression networks to identify genes that sit at the centre of these networks and interact with many other genes near ANM-associated variants. Such genes are analogous to the 'core' genes proposed in the omnigenic model of genetic architecture[18]. This approach identified 250 genes, 47 of which were within 300 kb of one of the identified 290 loci (Supplementary Tables 17, 18). A notable example is *MCM8*, which was implicated directly by two missense variants and is co-expressed with many genes highlighted by our GWAS (Extended Data Fig. 5).

ANM genes act across the life-course

Previous analyses have highlighted the involvement of DNA repair in the regulation of ovarian ageing. Our results support a much broader involvement of DDR and of metabolic signalling networks such as the phosphatidylinositol 3-kinase (PI3K)[19] pathway, and provides increased resolution of these pathways and when in the life-course they might act (Extended Data Fig. 1, Supplementary Results). We identified DDR pathways associated with replication stress, Fanconi anaemia, DNA–protein crosslink repair, R loops (Extended Data Fig. 6), meiotic recombination, and 58 genes implicated in the regulation of apoptosis (Supplementary Table 19), providing evidence that variation in cell death following DDR is an important mechanism of ANM. The products of the identified genes include components of and interactors with the central, conserved DDR checkpoint kinases ATR-CHEK1 (single-stranded DNA) and ATM-CHEK2 (double-strand breaks), which integrate and determine repair and cellular responses from a broad variety of DNA repair pathways (Extended Data Fig. 6). We observed differential expression of these genes across developmental stages in human follicles, further supporting the idea that they have distinct activities across fetal and follicular stages (Extended Data Fig. 7, Supplementary Table 20); for example, *TP63* was predominantly expressed during follicular stages, consistent with the induction of apoptosis in response to DNA damage observed in growing mouse oocytes[20–23]. These observations are consistent with the DDR regulating both the establishment of the ovarian reserve during fetal life and its depletion until ANM.

In utero effects and maternal diet

Previous work in mice has shown that a maternal obesogenic diet during pregnancy decreases the ovarian reserve in offspring[24]. We extend this observation by demonstrating that two of our highlighted genes (*Dmc1* and *Brsk1*) are differentially expressed in the ovaries of offspring from obese mice (Supplementary Table 5, Extended Data Fig. 8). *Dmc1* is a meiosis-specific DNA recombinase that assembles at the site of double-strand breaks and is essential for meiotic recombination and gamete formation[25]. The expression of *Brsk1* was decreased in ovarian tissue from the offspring of obese mice, and this effect appeared to be enhanced further when the offspring were also exposed to an obesogenic diet from weaning (Extended Data Fig. 8). *Brsk1* acts as a DNA damage sensor and targets *Wee1* and *Mapt1* for phosphorylation, both of which were also upregulated in our model. *Wee1* is highly expressed in fetal germ cells, inhibits mitosis and is specifically downregulated late in oogenesis[26]. The mechanisms that link maternal diet-induced altered expression of these genes to reduced ovarian reserve in the offspring remain unclear. However, our findings, in addition to observations that low birthweight is associated with early menopause[27], support the hypothesis that DDR mechanisms that act in utero to influence reproductive lifespan might be modified by maternal exposure.

Extending reproductive life in animals

Our GWAS highlighted LOF alleles in *CHEK2* associated with later ANM. Although previous work has shown that genetic manipulation of DDR genes in animal models reduces fertility and limits reproductive lifespan[28–30], it remains to be tested whether it can also extend it. CHEK2 has a crucial role in culling oocytes in mouse mutants that are defective in meiotic recombination or after artificial induction of double-strand breaks[22,31,32]. In young female mice, *Chek2* inactivation can partially rescue oocyte loss and, in some mutants, fertility, with high levels of non-physiologically induced endogenous and exogenous DNA damage[23,31,33,34]. To better understand the function of the checkpoint kinase pathways in physiological reproductive ageing, we used genetically modified *Chek1* and *Chek2* mice (Fig. 3, Extended Data Figs. 9–11). Follicular atresia was reduced in *Chek2*$^{-/-}$ females around reproductive senescence (13.5 months). This occurred without a concomitant increase in the ovarian reserve in young mice[31] (1.5 months) (Fig. 3a, Extended Data Fig. 9a–e). The aged *Chek2*$^{-/-}$ females showed elevated levels of anti-Müllerian hormone (Extended Data Fig. 9f) and an increased follicular response to gonadotrophin stimulation (Fig. 3c, Extended Data Fig. 9g), consistent with a larger ovarian reserve at 13.5 months. Fertilization, blastocyst formation and litter sizes in naturally mated aged *Chek2*$^{-/-}$ females were similar to those of littermate controls (Extended Data Fig. 9h–j), which suggests that the endogenous damage that *Chek2* responds to does not compromise the health of offspring or mothers in later reproductive life (Extended Data Fig. 9j, k). Thus, depletion of the ovarian reserve is slowed in *Chek2*$^{-/-}$ females, resulting in improved ovarian function around the time of reproductive senescence. This suggests a potential therapeutic target for enhancing ovarian stimulation in women undergoing in vitro fertilization (IVF) treatment through short-term apoptotic inhibition.

In contrast to *Chek2*$^{-/-}$ mice, *Chek1*$^{-/-}$ mice die as embryos due to the essential function of CHEK1 when DNA replication is perturbed as well as during mitosis[35]. We found that two different maternal, germline-specific conditional knockouts of *Chek1*, one of which also leads to

defects in prospermatogonia in males[36], resulted in infertility in females due to failure during preimplantation embryo development (Extended Data Fig. 10). CHEK1 is required for prophase I arrest and functions in G2/M checkpoint regulation in mouse oocytes[23,37] and its activator, ATR, is important for meiotic recombination as well as follicle formation[38,39]. An extra copy (resulting in three alleles) of mouse *Chek1* (*SuperChek1* or *sChek1*) has been reported to partially rescue lifespan in *ATR*^{Seckel} mice, which suggests that CHEK1 becomes rate-limiting when cells are under replication stress[40]. We found that *sChek1* on its own increased the ovarian reserve from birth as well as later in life (Fig. 3b, Extended Data Fig. 11b–f). Large antral follicle counts were also elevated in aged *sChek1* females, compared to littermate controls, indicating that follicular activity was also increased. Immediately before the typical age at reproductive senescence (11–13 months), *sChek1* females ovulated an increased number of mature MII oocytes in response to gonadotrophin stimulation (Fig. 3c, Extended Data Fig. 11g). These oocytes showed increased mRNA expression of *Chek1* (Extended Data Fig. 11a) and had a similar capacity for forming blastocyst embryos to wild-type oocytes (Extended Data Fig. 11i, j). When transferred, these embryos gave rise to healthy, fertile pups over two generations (Extended Data Fig. 11k–n). Thus, *sChek1* causes a larger ovarian reserve to be established at birth and the oocytes appear to maintain their genomic integrity, as confirmed by aneuploidy analysis, efficiency of embryogenesis and fertility of pups (Extended Data Fig. 11g–n), resulting in enhanced follicular activity and delayed reproductive senescence. We speculate that this is due to the upregulation of replication-associated DNA repair processes during mitosis and meiosis, and that repair might be limiting for establishing and maintaining the ovarian reserve. Together, our data show that modulation of key DDR genes can extend reproductive lifespan in vivo, generating healthy pups that are fertile over several generations. This can occur either by abolishing DDR checkpoints (*Chek2* deletion) or by upregulating repair processes (*sChek1*).

Health consequences of later ANM

We used our identified genetic variants and a Mendelian randomization framework to infer causal relationships between ANM and several health outcomes (Supplementary Tables 21–23). Consistent with previous studies[2,13], each one-year genetically mediated delay in ANM increased the relative risks of several hormone-sensitive cancers by up to 5% (Supplementary Table 21). By contrast, genetically mediated delays in ANM were beneficial for bone mineral density, fracture risk and risk of type 2 diabetes. Our findings are consistent with evidence from randomized controlled trials that oestrogen therapy maintains bone health and protects against type 2 diabetes[41,42]. Furthermore, recent Mendelian randomization studies have demonstrated causal associations between sex hormone levels and type 2 diabetes[43]. Trial data in younger women taking HRT suggested no increased risk of cardiovascular disease, stroke or all-cause mortality[42]. In agreement with these data, we found no evidence to support causal associations between ANM and cardiovascular disease, lipid levels, Alzheimer's disease, body mass or longevity (Supplementary Table 21), all of which have been reported in observational studies[44–50]. Finally, we evaluated putative modifiable determinants of ANM reported by observational studies[27]. We found that genetically mediated increases in alcohol consumption and tobacco smoking were associated with earlier ANM (Supplementary Tables 24, 25). Each additional cigarette smoked per day decreased ANM by about 2.5 weeks, and women who drank alcohol at the maximum recommended limit experienced menopause around 1 year earlier than those who drank little. Furthermore, genetically mediated age at menarche was associated with a decrease in ANM of about 8 weeks per year of earlier menarche.

Collectively, our findings provide insights into the biological processes of reproductive ageing in women, how they can be manipulated to extend reproductive life, and what the consequences of this might be at a population level. We anticipate that these findings will inform experimental studies seeking to identify new therapies for enhancing reproductive function and preserving fertility in women.

Online content

Any methods, additional references, Nature Research reporting summaries, source data, extended data, supplementary information, acknowledgements, peer review information; details of author contributions and competing interests; and statements of data and code availability are available at https://doi.org/10.1038/s41586-021-03779-7.

1. Lambalk, C. B., van Disseldorp, J., de Koning, C. H. & Broekmans, F. J. Testing ovarian reserve to predict age at menopause. *Maturitas* **63**, 280–291 (2009).
2. Collaborative Group on Hormonal Factors in Breast Cancer. Type and timing of menopausal hormone therapy and breast cancer risk: individual participant meta-analysis of the worldwide epidemiological evidence. *Lancet* **394**, 1159–1168 (2019).
3. Murray, A. et al. Population-based estimates of the prevalence of FMR1 expansion mutations in women with early menopause and primary ovarian insufficiency. *Genet. Med.* **16**, 19–24 (2014).
4. Christensen, K., Doblhammer, G., Rau, R. & Vaupel, J. W. Ageing populations: the challenges ahead. *Lancet* **374**, 1196–1208 (2009).
5. InterLACE Study Team. Variations in reproductive events across life: a pooled analysis of data from 505 147 women across 10 countries. *Hum. Reprod.* **34**, 881–893 (2019).
6. Gruhn, J. R. et al. Chromosome errors in human eggs shape natural fertility over reproductive life span. *Science* **365**, 1466–1469 (2019).
7. Donnez, J. & Dolmans, M.-M. Fertility preservation in women. *N. Engl. J. Med.* **377**, 1657–1665 (2017).
8. Yding Andersen, C., Mamsen, L. S. & Kristensen, S. G. Fertility preservation: freezing of ovarian tissue and clinical opportunities. *Reproduction* **158**, F27–F34 (2019).
9. Argyle, C. E., Harper, J. C. & Davies, M. C. Oocyte cryopreservation: where are we now? *Hum. Reprod. Update* **22**, 440–449 (2016).
10. Stolk, L. et al. Meta-analyses identify 13 loci associated with age at menopause and highlight DNA repair and immune pathways. *Nat. Genet.* **44**, 260–268 (2012).
11. Venturella, R. et al. The genetics of non-syndromic primary ovarian insufficiency: a systematic review. *Int. J. Fertil. Steril.* **13**, 161–168 (2019).
12. Titus, S. et al. Impairment of BRCA1-related DNA double-strand break repair leads to ovarian aging in mice and humans. *Sci. Transl. Med.* **5**, 172ra21 (2013).
13. Day, F. R. et al. Large-scale genomic analyses link reproductive aging to hypothalamic signaling, breast cancer susceptibility and BRCA1-mediated DNA repair. *Nat. Genet.* **47**, 1294–1303 (2015).
14. Horikoshi, M. et al. Elucidating the genetic architecture of reproductive ageing in the Japanese population. *Nat. Commun.* **9**, 1977 (2018).
15. Caburet, S. et al. Homozygous hypomorphic *BRCA2* variant in primary ovarian insufficiency without cancer or Fanconi anaemia trait. *J. Med. Genet.* **58**,125–134 (2020).
16. Thompson, D. J. et al. Genetic predisposition to mosaic Y chromosome loss in blood. *Nature* **575**, 652–657 (2019).
17. Day, F. R. et al. Genomic analyses identify hundreds of variants associated with age at menarche and support a role for puberty timing in cancer risk. *Nat. Genet.* **49**, 834–841 (2017).
18. Boyle, E. A., Li, Y. I. & Pritchard, J. K. An expanded view of complex traits: from polygenic to omnigenic. *Cell* **169**, 1177–1186 (2017).
19. Reddy, P. et al. Oocyte-specific deletion of *Pten* causes premature activation of the primordial follicle pool. *Science* **319**, 611–613 (2008).
20. Suh, E.-K. et al. p63 protects the female germ line during meiotic arrest. *Nature* **444**, 624–628 (2006).
21. Deutsch, G. B. et al. DNA damage in oocytes induces a switch of the quality control factor TAp63α from dimer to tetramer. *Cell* **144**, 566–576 (2011).
22. Tuppi, M. et al. Oocyte DNA damage quality control requires consecutive interplay of CHK2 and CK1 to activate p63. *Nat. Struct. Mol. Biol.* **25**, 261–269 (2018).
23. Rinaldi, V. D., Bloom, J. C. & Schimenti, J. C. Oocyte elimination through DNA damage signaling from CHK1/CHK2 to p53 and p63. *Genetics* **215**, 373–378 (2020).
24. Aiken, C. E., Tarry-Adkins, J. L., Penfold, N. C., Dearden, L. & Ozanne, S. E. Decreased ovarian reserve, dysregulation of mitochondrial biogenesis, and increased lipid peroxidation in female mouse offspring exposed to an obesogenic maternal diet. *FASEB J.* **30**, 1548–1556 (2016).
25. Pittman, D. L. et al. Meiotic prophase arrest with failure of chromosome synapsis in mice deficient for Dmc1, a germline-specific RecA homolog. *Mol. Cell* **1**, 697–705 (1998).
26. Nakajo, N. et al. Absence of Wee1 ensures the meiotic cell cycle in *Xenopus* oocytes. *Genes Dev.* **14**, 328–338 (2000).
27. Ruth, K. S. et al. Events in early life are associated with female reproductive ageing: a UK Biobank study. *Sci. Rep.* **6**, 24710 (2016).
28. Pan, Y. et al. A heterozygous hypomorphic mutation of Fanca causes impaired follicle development and subfertility in female mice. *Mol. Genet. Genomics* **296**, 103–112 (2021).
29. Bakker, S. T. et al. Fancm-deficient mice reveal unique features of Fanconi anemia complementation group M. *Hum. Mol. Genet.* **18**, 3484–3495 (2009).
30. Caburet, S. et al. Mutant cohesin in premature ovarian failure. *N. Engl. J. Med.* **370**, 943–949 (2014).
31. Bolcun-Filas, E., Rinaldi, V. D., White, M. E. & Schimenti, J. C. Reversal of female infertility by *Chk2* ablation reveals the oocyte DNA damage checkpoint pathway. *Science* **343**, 533–536 (2014).
32. Adhikari, D. et al. Inhibitory phosphorylation of Cdk1 mediates prolonged prophase I arrest in female germ cells and is essential for female reproductive lifespan. *Cell Res.* **26**, 1212–1225 (2016).

33. Rinaldi, V. D., Bolcun-Filas, E., Kogo, H., Kurahashi, H. & Schimenti, J. C. The DNA damage checkpoint eliminates mouse oocytes with chromosome synapsis failure. *Mol. Cell* **67**, 1026–1036.e2 (2017).
34. Tharp, M. E., Malki, S. & Bortvin, A. Maximizing the ovarian reserve in mice by evading LINE-1 genotoxicity. *Nat. Commun*. **11**, 330 (2020).
35. Liu, Q. et al. Chk1 is an essential kinase that is regulated by Atr and required for the G_2/M DNA damage checkpoint. *Genes Dev*. **14**, 1448–1459 (2000).
36. Abe, H. et al. CHEK1 coordinates DNA damage signaling and meiotic progression in the male germline of mice. *Hum. Mol. Genet*. **27**, 1136–1149 (2018).
37. Chen, L. et al. Checkpoint kinase 1 is essential for meiotic cell cycle regulation in mouse oocytes. *Cell Cycle* **11**, 1948–1955 (2012).
38. Pacheco, S. et al. ATR is required to complete meiotic recombination in mice. *Nat. Commun*. **9**, 2622 (2018).
39. Pacheco, S., Maldonado-Linares, A., Garcia-Caldés, M. & Roig, I. ATR function is indispensable to allow proper mammalian follicle development. *Chromosoma* **128**, 489–500 (2019).
40. López-Contreras, A. J., Gutierrez-Martinez, P., Specks, J., Rodrigo-Perez, S. & Fernandez-Capetillo, O. An extra allele of *Chk1* limits oncogene-induced replicative stress and promotes transformation. *J. Exp. Med*. **209**, 455–461 (2012).
41. Salpeter, S. R. et al. Meta-analysis: effect of hormone-replacement therapy on components of the metabolic syndrome in postmenopausal women. *Diabetes Obes. Metab*. **8**, 538–554 (2006).
42. Manson, J. E. et al. Menopausal hormone therapy and health outcomes during the intervention and extended poststopping phases of the Women's Health Initiative randomized trials. *J. Am. Med. Assoc*. **310**, 1353–1368 (2013).
43. Ruth, K. S. et al. Using human genetics to understand the disease impacts of testosterone in men and women. *Nat. Med*. **26**, 252–258 (2020).
44. Dam, V. et al. Association of menopausal characteristics and risk of coronary heart disease: a pan-European case-cohort analysis. *Int. J. Epidemiol*. **48**, 1275–1285 (2019).
45. de Kat, A. C. et al. Unraveling the associations of age and menopause with cardiovascular risk factors in a large population-based study. *BMC Med*. **15**, 2 (2017).
46. Atsma, F., Bartelink, M.-L. E. L., Grobbee, D. E. & van der Schouw, Y. T. Postmenopausal status and early menopause as independent risk factors for cardiovascular disease: a meta-analysis. *Menopause* **13**, 265–279 (2006).
47. Ambikairajah, A., Walsh, E. & Cherbuin, N. Lipid profile differences during menopause: a review with meta-analysis. *Menopause* **26**, 1327–1333 (2019).
48. Pike, C. J. Sex and the development of Alzheimer's disease. *J. Neurosci. Res*. **95**, 671–680 (2017).
49. Zhu, D. et al. Body mass index and age at natural menopause: an international pooled analysis of 11 prospective studies. *Eur. J. Epidemiol*. **33**, 699–710 (2018).
50. Shadyab, A. H. et al. Ages at menarche and menopause and reproductive lifespan as predictors of exceptional longevity in women: the Women's Health Initiative. *Menopause* **24**, 35–44 (2017).

Katherine S. Ruth[1,191], Felix R. Day[2,191], Jazib Hussain[3,191], Ana Martínez-Marchal[4,5,191], Catherine E. Aiken[6,7], Ajuna Azad[3], Deborah J. Thompson[8], Lucie Knoblochova[9,10], Hironori Abe[11], Jane L. Tarry-Adkins[6,7], Javier Martin Gonzalez[12], Pierre Fontanillas[13], Annique Claringbould[14], Olivier B. Bakker[15], Patrick Sulem[16], Robin G. Walters[17,18], Chikashi Terao[19,20,21], Sandra Turon[22], Momoko Horikoshi[23], Kuang Lin[17], N. Charlotte Onland-Moret[24], Aditya Sankar[3], Emil Peter Thrane Hertz[3,25], Pascal N. Timshel[26], Vallari Shukla[3], Rehannah Borup[3], Kristina W. Olsen[3,27], Paula Aguilera[3,28], Mònica Ferrer-Roda[4,5], Yan Huang[4,5], Stasa Stankovic[2], Paul R. H. J. Timmers[29,30], Thomas U. Ahearn[31], Behrooz Z. Alizadeh[32], Elnaz Naderi[32], Irene L. Andrulis[33,34], Alice M. Arnold[35], Kristan J. Aronson[36,37], Annelie Augustinsson[38], Stefania Bandinelli[39], Caterina M. Barbieri[40], Robin N. Beaumont[1], Heiko Becher[41], Matthias W. Beckmann[42], Stefania Benonisdottir[16], Sven Bergmann[43,44], Murielle Bochud[45], Eric Boerwinkle[46], Stig E. Bojesen[47,48,49], Manjeet K. Bolla[8], Dorret I. Boomsma[50,51,52], Nicholas Bowker[2], Jennifer A. Brody[53], Linda Broer[54], Julie E. Buring[55,56], Archie Campbell[57], Harry Campbell[29], Jose E. Castelao[58], Eulalia Catamo[59], Stephen J. Chanock[31], Georgia Chenevix-Trench[60], Marina Ciullo[61,62], Tanguy Corre[43,44,45], Fergus J. Couch[63], Angela Cox[64], Laura Crisponi[65], Simon S. Cross[66], Francesco Cucca[65,67], Kamila Czene[68], George Davey Smith[69,70], Eco J. C. N. de Geus[50,51,52], Renée de Mutsert[71], Immaculata De Vivo[72,73], Ellen W. Demerath[74], Joe Dennis[8], Alison M. Dunning[75], Miriam Dwek[76], Mikael Eriksson[77], Tõnu Esko[78,79], Peter A. Fasching[42,80], Jessica D. Faul[81], Luigi Ferrucci[82], Nora Franceschini[83], Timothy M. Frayling[1], Manuela Gago-Dominguez[84,85], Massimo Mezzavilla[86], Montserrat García-Closas[31], Christian Gieger[87,88,89], Graham G. Giles[90,91,92], Harald Grallert[87,88,89], Daniel F. Gudbjartsson[16], Vilmundur Gudnason[93,94], Pascal Guénel[95], Christopher A. Haiman[96], Niclas Håkansson[97], Per Hall[68], Caroline Hayward[30], Chunyan He[98,99], Wei He[77], Gerardo Heiss[83], Miya K. Høffding[3], John L. Hopper[91], Jouke J. Hottenga[50,51,52], Frank Hu[72,73,100], David Hunter[17,73,100,101,102], Mohammad A. Ikram[103], Rebecca D. Jackson[104], Micaella D. R. Joaquim[1], Esther M. John[105,106], Peter K. Joshi[29], David Karasik[56,107], Sharon L. R. Kardia[108], Christiana Kartsonaki[17,18], Robert Karlsson[109], Cari M. Kitahara[110], Ivana Kolcic[111], Charles Kooperberg[112], Peter Kraft[72,113], Allison W. Kurian[105,106], Zoltan Kutalik[44,45], Martina La Bianca[59], Genevieve LaChance[114], Claudia Langenberg[2], Lenore J. Launer[115], Joop S. E. Laven[116], Deborah A. Lawlor[69,70], Loic Le Marchand[117], Jingmei Li[68], Annika Lindblom[118,119], Sara Lindstrom[120], Tricia Lindstrom[121], Martha Linet[110], YongMei Liu[122], Simin Liu[123,124], Jian'an Luan[2], Reedik Mägi[79], Patrik K. E. Magnusson[109], Massimo Mangino[114,125], Arto Mannermaa[126,127,128], Brumat Marco[86], Jonathan Marten[30], Nicholas G. Martin[129], Hamdi Mbarek[50,51,52], Barbara McKnight[35], Sarah E. Medland[129], Christa Meisinger[88,130], Thomas Meitinger[131], Cristina Menni[114], Andres Metspalu[79], Lili Milani[79], Roger L. Milne[90,91,92], Grant W. Montgomery[132], Dennis O. Mook-Kanamori[71,133], Antonella Mulas[65], Anna M. Mulligan[134,135], Alison Murray[136], Mike A. Nalls[137], Anne Newman[138,139], Raymond Noordam[140], Teresa Nutile[61], Dale R. Nyholt[141], Andrew F. Olshan[142], Håkan Olsson[38], Jodie N. Painter[129], Alpa V. Patel[143], Nancy L. Pedersen[109], Natalia Perjakova[79], Annette Peters[88,89], Ulrike Peters[112], Paul D. P. Pharoah[8,75], Ozren Polasek[144,145], Eleonora Porcu[65], Bruce M. Psaty[53], Iffat Rahman[146], Gad Rennert[147], Hedy S. Rennert[147], Paul M. Ridker[55,56], Susan M. Ring[69,70], Antonietta Robino[59], Lynda M. Rose[55], Frits R. Rosendaal[71], Jacques Rossouw[148], Igor Rudan[29], Rico Rueedi[43,44], Daniela Ruggiero[61,62], Cinzia F. Sala[40], Emmanouil Saloustros[149], Dale P. Sandler[150], Serena Sanna[65], Elinor J. Sawyer[151], Chloé Sarnowski[152], David Schlessinger[153], Marjanka K. Schmidt[154,155], Minouk J. Schoemaker[156], Katharina E. Schraut[29,157], Christopher Scott[121], Saleh Shekari[1], Amruta Shrikhande[3], Albert V. Smith[93,94], Blair H. Smith[158], Jennifer A. Smith[108], Rossella Sorice[61], Melissa C. Southey[90,92,159], Tim D. Spector[114], John J. Spinelli[160,161], Meir Stampfer[72,73,100], Doris Stöckl[88,162], Joyce B. J. van Meurs[54], Konstantin Strauch[163,164,165], Unnur Styrkarsdottir[16], Anthony J. Swerdlow[156,166], Toshiko Tanaka[82], Lauren R. Teras[143], Alexander Teumer[167], Unnur Þorsteinsdottir[16,168], Nicholas J. Timpson[69,70], Daniela Toniolo[40], Michela Traglia[40], Melissa A. Troester[142], Thérèse Truong[95], Jessica Tyrrell[1], André G. Uitterlinden[54,103], Sheila Ulivi[59], Celine M. Vachon[169], Veronique Vitart[30], Uwe Völker[170], Peter Vollenweider[171], Henry Völzke[167], Qin Wang[8], Nicholas J. Wareham[2], Clarice R. Weinberg[172], David R. Weir[81], Amber N. Wilcox[31], Ko Willems van Dijk[173,174,175], Gonneke Willemsen[50,51,52], James F. Wilson[29,30], Bruce H. R. Wolffenbuttel[176], Alicja Wolk[97,177], Andrew R. Wood[1], Wei Zhao[108], Marek Zygmunt[178], Biobank-based Integrative Omics Study (BIOS) Consortium*, eQTLGen Consortium*, The Biobank Japan Project*, China Kadoorie Biobank Collaborative Group*, kConFab Investigators*, The LifeLines Cohort Study*, The InterAct consortium*, 23andMe Research Team*, Zhengming Chen[17,18], Liming Li[179,180], Lude Franke[15,181], Stephen Burgess[182,183], Patrick Deelen[15,184], Tune H. Pers[26], Marie Louise Grøndahl[27], Claus Yding Andersen[185], Anna Pujol[22], Andres J. Lopez-Contreras[3,28], Jeremy A. Daniel[25], Kari Stefansson[16,168], Jenny Chang-Claude[186,187], Yvonne T. van der Schouw[24], Kathryn L. Lunetta[152,188], Daniel I. Chasman[55,56], Douglas F. Easton[8,75], Jenny A. Visser[54], Susan E. Ozanne[6], Satoshi H. Namekawa[11], Petr Solc[9,193], Joanne M. Murabito[188,189], Ken K. Ong[2,190], Eva R. Hoffmann[3,192]✉, Anna Murray[1,192]✉, Ignasi Roig[4,5,192]✉ & John R. B. Perry[2,54,192]✉

[1]Genetics of Human Complex Traits, University of Exeter Medical School, University of Exeter, Exeter, UK. [2]MRC Epidemiology Unit, University of Cambridge School of Clinical Medicine, Institute of Metabolic Science, Cambridge Biomedical Campus, Cambridge, UK. [3]DNRF Center for Chromosome Stability, Department of Cellular and Molecular Medicine, Faculty of Health and Medical Sciences, University of Copenhagen, Copenhagen, Denmark. [4]Genome Integrity and Instability Group, Institut de Biotecnologia i Biomedicina, Universitat Autònoma de Barcelona, Cerdanyola del Vallès, Spain. [5]Department of Cell Biology, Physiology and Immunology, Universitat Autònoma de Barcelona, Cerdanyola del Vallès, Spain. [6]University of Cambridge Metabolic Research Laboratories and MRC Metabolic Diseases Unit, Wellcome–MRC Institute of Metabolic Science, Addenbrooke's Hospital, Cambridge, UK. [7]Department of Obstetrics and Gynaecology, University of Cambridge, The Rosie Hospital and NIHR Cambridge Biomedical Research Centre, Cambridge, UK. [8]Centre for Cancer Genetic Epidemiology, Department of Public Health and Primary Care, University of Cambridge, Cambridge, UK. [9]Institute of Animal Physiology and Genetics of the Czech Academy of Sciences, Libechov, Czech Republic. [10]Faculty of Science, Charles University, Prague, Czech Republic. [11]Division of Reproductive Sciences, Cincinnati Children's Hospital Medical Center, Cincinnati, OH, USA. [12]Transgenic Core Facility, Department of Experimental Medicine, Faculty of Health and Medical Sciences, University of Copenhagen, Copenhagen, Denmark. [13]23andMe Inc., Sunnyvale, CA, USA. [14]Structural and Computational Biology Unit, EMBL, Heidelberg, Germany. [15]University of Groningen, University Medical Center Groningen, Department of Genetics, Groningen, The Netherlands. [16]deCODE genetics/Amgen, Reykjavik, Iceland. [17]Nuffield Department of Population Health, University of Oxford, Oxford, UK. [18]MRC Population Health Research Unit, University of Oxford, Oxford, UK. [19]Laboratory for Statistical and Translational Genetics, RIKEN Center for Integrative Medical Sciences, Yokohama, Japan. [20]Clinical Research Center, Shizuoka General Hospital, Shizuoka, Japan. [21]Department of Applied Genetics, School of Pharmaceutical Sciences, University of Shizuoka, Shizuoka, Japan. [22]Transgenic Animal Unit, Center of Animal Biotechnology and Gene Therapy, Universitat Autònoma de Barcelona, Cerdanyola del Vallès, Spain. [23]Laboratory for Genomics of Diabetes and Metabolism, RIKEN Center for Integrative Medical Sciences, Yokohama, Japan. [24]Julius Center for Health Sciences and Primary Care, University Medical Center Utrecht, Utrecht University, Utrecht, The Netherlands. [25]The Novo Nordisk Foundation Center for Protein Research, Faculty of Health and Medical Sciences, University of Copenhagen, Copenhagen, Denmark. [26]The Novo Nordisk Foundation Center for Basic Metabolic Research, Faculty of Health and Medical Sciences, University of Copenhagen, Copenhagen, Denmark. [27]Reproductive Medicine, Department of Obstetrics and Gynaecology, Herlev and Gentofte Hospital, Copenhagen University Hospital, Herlev, Denmark. [28]Centro Andaluz de Biología Molecular y Medicina Regenerativa (CABIMER), Consejo Superior de Investigaciones Científicas (CSIC) – Universidad de Sevilla –Universidad Pablo de Olavide, Seville, Spain. [29]Centre for Global Health Research, Usher Institute, University of Edinburgh, Edinburgh, UK. [30]MRC Human Genetics Unit, Institute of Genetics and Molecular Medicine, University of Edinburgh, Western General Hospital, Edinburgh, UK. [31]Division of Cancer Epidemiology and Genetics, National Cancer Institute, National Institutes of Health, Department of Health and Human Services, Bethesda, MD, USA. [32]Department of Epidemiology, University Medical Center Groningen, University of Groningen, Groningen, The Netherlands. [33]Fred A. Litwin Center for Cancer Genetics, Lunenfeld-Tanenbaum Research Institute of Mount Sinai Hospital, Toronto, Ontario, Canada. [34]Department of Molecular Genetics, University of Toronto, Toronto, Ontario, Canada. [35]Department of Biostatistics, University of Washington, Seattle, WA, USA. [36]Department of Public Health Sciences, Queen's University, Kingston, Ontario, Canada. [37]Cancer Research Institute, Queen's University, Kingston, Ontario, Canada. [38]Department of Cancer Epidemiology, Clinical Sciences, Lund University, Lund, Sweden. [39]Geriatric Unit, Azienda Sanitaria Firenze (ASF), Florence, Italy. [40]Genetics of Common Disorders Unit, IRCCS San Raffaele Scientific Institute, Milan, Italy. [41]Institute of Medical Biometry and Epidemiology, University Medical Center Hamburg-Eppendorf, Hamburg, Germany. [42]Department of Gynecology and Obstetrics, Comprehensive Cancer Center ER-EMN, University Hospital Erlangen, Friedrich-Alexander-University Erlangen-Nuremberg, Erlangen, Germany. [43]Department of Computational Biology, University of Lausanne, Lausanne, Switzerland. [44]Swiss Institute of Bioinformatics, Lausanne, Switzerland. [45]University Center for Primary Care and Public Health, University of Lausanne, Lausanne, Switzerland. [46]Human Genetics Center, School of Public Health, The University of Texas Health Science Center at Houston, Houston, TX, USA. [47]Copenhagen General Population Study, Herlev and Gentofte Hospital, Copenhagen University Hospital, Herlev, Denmark. [48]Department of Clinical Biochemistry, Herlev and Gentofte Hospital, Copenhagen University Hospital, Herlev, Denmark. [49]Faculty of Health and Medical Sciences, University of Copenhagen, Copenhagen, Denmark. [50]Department of Biological Psychology, Vrije Universiteit Amsterdam, Amsterdam, The Netherlands. [51]Amsterdam Public Health (APH) Research Institute, Amsterdam, The Netherlands. [52]Amsterdam Reproduction and Development (AR&D) Research Institute, Amsterdam, The Netherlands. [53]Cardiovascular Health Research Unit, Departments of Medicine, Epidemiology, and Health Services, University of Washington, Seattle, WA, USA. [54]Department of Internal Medicine, Erasmus MC, Rotterdam, The Netherlands. [55]Brigham and Women's Hospital, Boston, MA, USA. [56]Harvard Medical School, Boston, MA, USA. [57]Medical Genetics Section, Centre for Genomic and Experimental Medicine, Institute of Genetics and Molecular Medicine, University of Edinburgh, Edinburgh, UK. [58]Oncology and Genetics Unit, Instituto de Investigacion Sanitaria Galicia Sur (IISGS), Xerencia de Xestion Integrada de Vigo-SERGAS, Vigo, Spain. [59]Institute for Maternal and Child Health – IRCCS 'Burlo Garofolo', Trieste, Italy. [60]Department of Genetics and Computational Biology, QIMR Berghofer Medical Research Institute, Brisbane, Queensland, Australia. [61]Institute of Genetics and Biophysics – CNR, Naples, Italy. [62]IRCCS Neuromed, Pozzilli, Isernia, Italy. [63]Department of Laboratory Medicine and Pathology, Mayo Clinic, Rochester, MN, USA. [64]Sheffield Institute for Nucleic Acids (SInFoNiA), Department of Oncology and Metabolism, University of Sheffield, Sheffield, UK. [65]Institute of Genetics and Biomedical Research, National Research Council, Cagliari,

Italy. [66]Academic Unit of Pathology, Department of Neuroscience, University of Sheffield, Sheffield, UK. [67]University of Sassari, Department of Biomedical Sciences, Sassari, Italy. [68]Karolinska Institutet, Department of Medical Epidemiology and Biostatistics, Stockholm, Sweden. [69]MRC Integrative Epidemiology Unit, University of Bristol, Bristol, UK. [70]Population Health Science, Bristol Medical School, University of Bristol, Bristol, UK. [71]Department of Clinical Epidemiology, Leiden University Medical Center, Leiden, The Netherlands. [72]Department of Epidemiology, Harvard T. H. Chan School of Public Health, Boston, MA, USA. [73]Channing Division of Network Medicine, Department of Medicine, Brigham and Women's Hospital and Harvard Medical School, Boston, MA, USA. [74]Division of Epidemiology & Community Health, University of Minnesota, Minneapolis, MN, USA. [75]Centre for Cancer Genetic Epidemiology, Department of Oncology, University of Cambridge, Cambridge, UK. [76]School of Life Sciences, University of Westminster, London, UK. [77]Department of Medical Epidemiology and Biostatistics, Karolinska Institutet, Stockholm, Sweden. [78]Population and Medical Genetics, Broad Institute, Cambridge, MA, USA. [79]Estonian Genome Center, Institute of Genomics, University of Tartu, Tartu, Estonia. [80]David Geffen School of Medicine, Department of Medicine, Division of Hematology and Oncology, University of California at Los Angeles, Los Angeles, CA, USA. [81]Survey Research Center, Institute for Social Research, Ann Arbor, MI, USA. [82]Translational Gerontology Branch, National Institute on Aging, Baltimore, MD, USA. [83]Department of Epidemiology, Gillings School of Global Public Health, University of North Carolina, Chapel Hill, NC, USA. [84]Fundación Pública Galega de Medicina Xenómica, Instituto de Investigación Sanitaria de Santiago de Compostela (IDIS), Complejo Hospitalario Universitario de Santiago, SERGAS, Santiago de Compostela, Spain. [85]Moores Cancer Center, University of California San Diego, La Jolla, CA, USA. [86]Department of Medical Sciences, University of Trieste, Trieste, Italy. [87]Research Unit of Molecular Epidemiology, Helmholtz Zentrum München–German Research Center for Environmental Health, Neuherberg, Germany. [88]Institute of Epidemiology II, Helmholtz Zentrum München–German Research Center for Environmental Health, Neuherberg, Germany. [89]German Center for Diabetes Research (DZD), Neuherberg, Germany. [90]Cancer Epidemiology Division, Cancer Council Victoria, Melbourne, Victoria, Australia. [91]Centre for Epidemiology and Biostatistics, Melbourne School of Population and Global Health, The University of Melbourne, Melbourne, Victoria, Australia. [92]Precision Medicine, School of Clinical Sciences at Monash Health, Monash University, Clayton, Victoria, Australia. [93]Icelandic Heart Association, Kopavogur, Iceland. [94]Faculty of Medicine, University of Iceland, Reykjavik, Iceland. [95]Cancer & Environment Group, Center for Research in Epidemiology and Population Health (CESP), INSERM, University Paris-Sud, University Paris-Saclay, Villejuif, France. [96]Department of Preventive Medicine, Keck School of Medicine, University of Southern California, Los Angeles, CA, USA. [97]Institute of Environmental Medicine, Karolinska Institutet, Stockholm, Sweden. [98]Division of Medical Oncology, Department of Internal Medicine, University of Kentucky College of Medicine, Lexington, KY, USA. [99]The Cancer Prevention and Control Research Program, University of Kentucky Markey Cancer Center, Lexington, KY, USA. [100]Department of Nutrition, Harvard T. H. Chan School of Public Health, Boston, MA, USA. [101]Department of Epidemiology, Harvard T. H. Chan School of Public Health, Boston, MA, USA. [102]Broad Institute of Harvard and MIT, Cambridge, MA, USA. [103]Department of Epidemiology, Erasmus MC, Rotterdam, The Netherlands. [104]Department of Internal Medicine, The Ohio State University, Columbus, OH, USA. [105]Department of Epidemiology & Population Health, Stanford University School of Medicine, Stanford, CA, USA. [106]Department of Medicine, Division of Oncology, Stanford Cancer Institute, Stanford University School of Medicine, Stanford, CA, USA. [107]Hebrew SeniorLife Institute for Aging Research, Boston, MA, USA. [108]Department of Epidemiology, School of Public Health, University of Michigan, Ann Arbor, MI, USA. [109]Department of Medical Epidemiology and Biostatistics, Karolinska Institutet, Stockholm, Sweden. [110]Radiation Epidemiology Branch, Division of Cancer Epidemiology and Genetics, National Cancer Institute, Bethesda, MD, USA. [111]Faculty of Medicine, University of Split, Split, Croatia. [112]Division of Public Health Sciences, Fred Hutchinson Cancer Research Center, Seattle, WA, USA. [113]Department of Biostatistics, Harvard T. H. Chan School of Public Health, Boston, MA, USA. [114]Department of Twin Research and Genetic Epidemiology, King's College London, London, UK. [115]Laboratory of Epidemiology and Population Sciences, National Institute on Aging, Intramural Research Program, National Institutes of Health, Bethesda, MD, USA. [116]Division of Reproductive Endocrinology and Infertility, Department of Obstetrics and Gynecology, Erasmus University Medical Center, Rotterdam, The Netherlands. [117]Epidemiology Program, University of Hawaii Cancer Center, Honolulu, HI, USA. [118]Department of Molecular Medicine and Surgery, Karolinska Institutet, Stockholm, Sweden. [119]Department of Clinical Genetics, Karolinska University Hospital, Stockholm, Sweden. [120]Department of Epidemiology, University of Washington, Seattle, WA, USA. [121]Department of Health Sciences Research, Mayo Clinic, Rochester, MN, USA. [122]Center for Human Genetics, Division of Public Health Sciences, Wake Forest School of Medicine, Wake Forest, NC, USA. [123]Department of Epidemiology, Brown University, Providence, RI, USA. [124]Department of Medicine, Brown University, Providence, RI, USA. [125]NIHR Biomedical Research Centre at Guy's and St. Thomas' Foundation Trust, London, UK. [126]Translational Cancer Research Area, University of Eastern Finland, Kuopio, Finland. [127]Institute of Clinical Medicine, Pathology and Forensic Medicine, University of Eastern Finland, Kuopio, Finland. [128]Biobank of Eastern Finland, Kuopio University Hospital, Kuopio, Finland. [129]QIMR Berghofer Medical Research Insititute, Brisbane, Queensland, Australia. [130]Central Hospital of Augsburg, MONICA/KORA Myocardial Infarction Registry, Augsburg, Germany. [131]Institute of Human Genetics, Helmholtz Zentrum München, German Research Center for Environmental Health, Neuherberg, Germany. [132]Institute for Molecular Bioscience, The University of Queensland, Brisbane, Queensland, Australia. [133]Department of Public Health and Primary Care, Leiden University Medical Center, Leiden, The Netherlands. [134]Department of Laboratory Medicine and Pathobiology, University of Toronto, Toronto, Ontario, Canada. [135]Laboratory Medicine Program, University Health Network, Toronto, Ontario, Canada. [136]The Institute of Medical Sciences, Aberdeen Biomedical Imaging Centre, University of Aberdeen, Aberdeen, UK. [137]Laboratory of Neurogenetics, National Institute on Aging, National Institutes of Health, Bethesda, MD, USA. [138]Department of Epidemiology, University of Pittsburgh, Pittsburgh, PA, USA. [139]Department of Medicine, University of Pittsburgh, Pittsburgh, PA, USA. [140]Department of Internal Medicine, Section of Gerontology and Geriatrics, Leiden University Medical Center, Leiden, The Netherlands. [141]Centre for Genomics and Personalised Health, School of Biomedical Sciences, Faculty of Health, Queensland University of Technology, Brisbane, Queensland, Australia. [142]Department of Epidemiology, Gillings School of Global Public Health and UNC Lineberger Comprehensive Cancer Center, University of North Carolina at Chapel Hill, Chapel Hill, NC, USA. [143]Department of Population Science, American Cancer Society, Atlanta, GA, USA. [144]Faculty of Medicine, University of Split, Split, Croatia. [145]Gen-Info Ltd, Zagreb, Croatia. [146]Quantify Research, Stockholm, Sweden. [147]Clalit National Cancer Control Center, Carmel Medical Center and Technion Faculty of Medicine, Haifa, Israel. [148]Women's Health Initiative Branch, National Heart, Lung, and Blood Institute, Bethesda, MD, USA. [149]Department of Oncology, University Hospital of Larissa, Larissa, Greece. [150]Epidemiology Branch, National Institute of Environmental Health Sciences, NIH, Research Triangle Park, NC, USA. [151]School of Cancer & Pharmaceutical Sciences, Comprehensive Cancer Centre, Guy's Campus, King's College London, London, UK. [152]Department of Biostatistics, Boston University School of Public Health, Boston, MA, USA. [153]National Institute on Aging, Intramural Research Program, Baltimore, MD, USA. [154]Division of Molecular Pathology, The Netherlands Cancer Institute – Antoni van Leeuwenhoek Hospital, Amsterdam, The Netherlands. [155]Division of Psychosocial Research and Epidemiology, The Netherlands Cancer Institute – Antoni van Leeuwenhoek Hospital, Amsterdam, The Netherlands. [156]Division of Genetics and Epidemiology, The Institute of Cancer Research, London, UK. [157]Centre for Cardiovascular Sciences, Queen's Medical Research Institute, University of Edinburgh, Royal Infirmary of Edinburgh, Edinburgh, UK. [158]Division of Population and Health Genomics, University of Dundee, Dundee, UK. [159]Department of Clinical Pathology, The University of Melbourne, Melbourne, Victoria, Australia. [160]Population Oncology, BC Cancer, Vancouver, British Columbia, Canada. [161]School of Population and Public Health, University of British Columbia, Vancouver, BC, Canada. [162]Department of Obstetrics and Gynaecology, Campus Grosshadern, Ludwig-Maximilians-Universität, Munich, Germany. [163]Institute of Genetic Epidemiology, Helmholtz Zentrum München – German Research Center for Environmental Health, Neuherberg, Germany. [164]Chair of Genetic Epidemiology, IBE, Faculty of Medicine, LMU Munich, Munich, Germany. [165]Institute of Medical Biostatistics, Epidemiology and Informatics (IMBEI), University Medical Center, Johannes Gutenberg University, Mainz, Germany. [166]Division of Breast Cancer Research, The Institute of Cancer Research, London, UK. [167]Institute for Community Medicine, University Medicine Greifswald, Greifswald, Germany. [168]Faculty of Medicine, School of Health Sciences, University of Iceland, Reykjavik, Iceland. [169]Department of Health Science Research, Division of Epidemiology, Mayo Clinic, Rochester, MN, USA. [170]Interfaculty Institute for Genetics and Functional Genomics, University Medicine Greifswald, Greifswald, Germany. [171]Department of Medicine, Internal Medicine, Lausanne University Hospital and University of Lausanne, Lausanne, Switzerland. [172]Biostatistics and Computational Biology Branch, National Institute of Environmental Health Sciences, NIH, Research Triangle Park, NC, USA. [173]Department of Internal Medicine, Division of Endocrinology, Leiden University Medical Center, Leiden, The Netherlands. [174]Einthoven Laboratory for Experimental Vascular Medicine, Leiden University Medical Center, Leiden, The Netherlands. [175]Department of Human Genetics, Leiden University Medical Center, Leiden, The Netherlands. [176]Department of Endocrinology, University Medical Center Groningen, University of Groningen, Groningen, The Netherlands. [177]Department of Surgical Sciences, Uppsala University, Uppsala, Sweden. [178]Department of Obstetrics and Gynecology, University Medicine Greifswald, Greifswald, Germany. [179]School of Public Health, Peking University Health Science Center, Beijing, P.R. China. [180]Peking University Center for Public Health and Epidemic Preparedness & Response, Beijing, P.R. China. [181]Oncode Institute, Utrecht, The Netherlands. [182]Department of Public Health and Primary Care, University of Cambridge, Cambridge, UK. [183]MRC Biostatistics Unit, University of Cambridge, Cambridge, UK. [184]Department of Genetics, University Medical Centre Utrecht, Utrecht, The Netherlands. [185]Laboratory of Reproductive Biology, The Juliane Marie Centre for Women, Children and Reproduction, Copenhagen University Hospital and Faculty of Health and Medical Sciences, University of Copenhagen, Copenhagen, Denmark. [186]Division of Cancer Epidemiology, German Cancer Research Center (DKFZ), Heidelberg, Germany. [187]Cancer Epidemiology Group, University Cancer Center Hamburg (UCCH), University Medical Center Hamburg-Eppendorf, Hamburg, Germany. [188]NHLBI's and Boston University's Framingham Heart Study, Framingham, MA, USA. [189]Boston University School of Medicine, Department of Medicine, Section of General Internal Medicine, Boston, MA, USA. [190]Department of Paediatrics, University of Cambridge, Cambridge, UK. [191]These authors contributed equally: Katherine S. Ruth, Felix R. Day, Jazib Hussain, Ana Martínez-Marchal. [192]These authors jointly supervised this work: Eva R. Hoffmann, Anna Murray, Ignasi Roig, John R. B. Perry. [193]Deceased.

Methods

Information on ethical regulations and approvals for all animal experiments are detailed in the corresponding sections below. Within each of the human population studies included in the genome-wide analyses (all of which have been previously published), each participant provided informed consent and the study protocol was approved by the institutional review board at the parent institution.

No statistical methods were used to predetermine sample size unless otherwise specified. The experiments were not randomized unless otherwise specified and investigators were not blinded to allocation during experiments and outcome assessment.

Phenotype definition

We included women with ANM from age 40 to 60 years inclusive. ANM was derived from self-reported questionnaire data by each study (Supplementary Table 1) and was the age at last naturally occurring menstrual period followed by at least 12 consecutive months of amenorrhea. Exclusions were women with menopause caused by hysterectomy, bilateral ovariectomy, radiation or chemotherapy, and those using HRT before menopause. Within each of the studies, each participant provided written informed consent and the study protocol was approved by the institutional review board at the parent institution.

Genome-wide association study meta-analysis

A genome-wide meta-analysis of autosomal and chromosome X variants in women of European ancestry was carried out on summary statistics from analyses in three strata, allowing for the identification of heterogeneity due to different methodology. The three strata were (Extended Data Fig. 2): (1) meta-analysis of 1000 Genomes imputed studies; (2) meta-analysis of samples from the Breast Cancer Association Consortium (BCAC: http://bcac.ccge.medschl.cam.ac.uk); (3) UK Biobank GWAS. The overall meta-analysis included variants present in at least two of the three strata. All meta-analyses were inverse-variance weighted without GC correction and were carried out in METAL (https://genome.sph.umich.edu/wiki/METAL_Documentation). Analysis was conducted by analysts at two geographically distinct sites independently and the resulting summary statistics were compared for consistency.

The meta-analysis of 1000 Genomes imputed studies included 40 datasets imputed to 1000 Genomes Phase I version 3 for the autosomes and 29 for chromosome X (Supplementary Table 1, Supplementary Notes). Each individual study applied quality control to directly genotyped variants and samples before imputation (suggested exclusion thresholds for variants were Hardy–Weinberg equilibrium $P < 1 \times 10^{-5}$, call rate <95% and MAF <1%; suggested exclusions for samples were >5% missing genotypes, population outliers, high inbreeding coefficient, heterozygosity outliers, sex mismatches and related samples). Each individual study carried out GWAS using a two-tailed additive linear regression model adjusted for genetic principal components/relationship matrix depending on the software used (Supplementary Table 1), without GC correction. As all samples included were female, chromosome X was analysed as for the autosomes. Once data were submitted, each study underwent quality control centrally according to standard protocols implemented independently by two analysts. Summary statistics for each study were stored centrally. Prior to meta-analysis, genetic variant IDs were converted to 'chr:position' format (position in build 37) and alleles for insertion/deletion polymorphisms were coded as 'I/D' to ensure consistency across studies. Meta-analysis was carried out including SNPs with imputation quality ≥ 0.4 and MAF ≥ 0.001. Variants in at least half of datasets for either the autosomes or for chromosome X (as appropriate) were taken forward to the overall meta-analysis, resulting in ~10.9 million variants.

GWAS summary statistics for the BCAC data were provided as four datasets, containing breast cancer cases and controls, with each genotyped on the iCOGs and OncoArray genotyping arrays (Supplementary Table 1). Quality control was applied to directly genotyped variants before imputation and data were imputed to the HRC r1.1 (2016) reference panel. Association analysis and quality control were carried out centrally as for the 1000 Genomes imputed studies. Summary statistics from the four BCAC datasets were meta-analysed, including variants with imputation quality ≥ 0.4 and MAF ≥ 0.001. Variants in two or more of the four datasets were taken forward to the overall meta-analysis, resulting in ~14.5 million variants.

UK Biobank genotyped 488,377 participants on two arrays: 49,950 on the UK BiLEVE Axiom array (807,411 markers) and 438,427 on the UK Biobank Axiom array (825,927 markers), which were then imputed using a combined 1000 Genomes Phase 3 and HRC reference panel. Details of central genotyping, quality control and imputation are described elsewhere[51]. We included 451,454 individuals identified as European in our analysis. In brief, principal components analyses were used to cluster individuals of white European descent (described more fully elsewhere[52]). We further removed participants who had subsequently withdrawn from the study ($n = 7$) and those for whom self-reported sex did not match genetic sex ($n = 348$), resulting in 451,099 individuals. GWAS was carried out in 106,048 women with ANM by applying a linear mixed model in BOLT-LMM[53] to adjust for population structure and relatedness, also adjusting for study centre and data release. Summary statistics taken forward to the overall meta-analyses were for ~16.6 million variants with imputation quality ≥ 0.5 and MAF ≥ 0.001. UK Biobank data were analysed by two analysts independently and summary statistics results were compared for consistency.

Genome-wide significance was set at $P < 5 \times 10^{-8}$. Statistical independence was determined using a combination of two approaches. First, we used distance-based clumping to select the most significantly associated SNP within a 1-Mb window. Second, we augmented this list with secondary signals within these 1-Mb windows that were identified through approximate conditional analysis implemented in GCTA[54]. We considered only secondary signals that were uncorrelated with other selected signals ($r^2 < 0.05$) and genome-wide significant in both univariate and joint models. Ten thousand ancestry-matched samples from the UK Biobank were used in GCTA as an LD reference panel.

Assessing the effect of time to event models on the signals identified

We performed Cox proportional hazards regression for the 290 genome-wide-significant ANM signals, allowing inclusion in our analyses of women excluded from the definition of natural menopause. We used UK Biobank imputed genotype data and performed analyses in 379,768 unrelated individuals of European descent (as previously described[52]), of whom 185,293 were included in our Cox analyses (phenotype definition as previously described[27]). In brief, Cox proportional hazards regression was run using stset and stcox (Breslow method for ties) in Stata v.16.0 using age as the time variable, starting at birth (0 years) and ending at last age at risk of natural menopause. Natural menopause was set as the event, with individuals censored at bilateral oophorectomy and/or hysterectomy, or start of HRT use (if ongoing at time of menopause, hysterectomy or oophorectomy). We included the covariates genotyping chip and release of genotype data, recruitment centre and the first five genetic principal components, which were considered to be constant throughout the time at risk. We calculated −1 × natural log(hazard ratio) to allow comparison with effect estimates from linear regression from the full meta-analysis and meta-analysis excluding UK Biobank.

Confirmation of identified signals and variance explained estimates

We sought to confirm our findings by testing the 290 identified loci in an independent sample of 294,828 women from 23andMe. Participants provided informed consent and participated in the research online, under

a protocol approved by the external AAHRPP-accredited IRB, Ethical & Independent Review Services (E&I Review). Participants were included in the analysis on the basis of consent status as checked at the time data analyses were initiated. The variant-level data for the 23andMe replication dataset are fully disclosed in the manuscript. Individual-level data are not publicly available because of participant confidentiality, and in accordance with the IRB-approved protocol under which the study was conducted. Women's age at menopause was ascertained across multiple surveys using two questions: "About how old were you when you had your last menstrual period? (under_30/30_34/45_49/40_44/55+/50_54/35_39/declined/not_sure)" and "How old were you when you had your last menstrual period?". As menopause age was ascertained in 4-year bins we rescaled the effect estimates appropriately to be on the same 1-year scale as our discovery analyses. Analyses were performed using a linear model (Gaussian family), controlling for age (in years), the top five genetic principal components and genotyping platform.

To assess the relevance of these loci in women of East Asian ancestry, we meta-analysed data (total $n = 78,317$ women) from the China Kadoorie Biobank study and Biobank Japan (BBJ). A total of 47,140 female participants in BBJ whose age at menopause was available were included in the current study. If different ages at menopause were reported at multiple visits, we took mean of ages at menopause. We excluded individuals (1) with maximum difference more than five years in the reported ages at menopause on multiple visits; (2) whose age at recruitment was younger than reported age at menopause; (3) whose age at menopause was younger than 40 or older than 60 years; and (4) with medical history of hysterectomy, ovariectomy, radiation, chemotherapy or hormone replacement treatment before age at menopause. Subjects (1) whose DNA microarray data was not available, (2) with low call rate (<0.98), (3) whose genetic data suggested as male, (4) who were genetically identical to other subjects or (5) who were outliers from the EAS cluster in the PCA plot were excluded from the analyses. We applied the same quality control for variants as the previous literature[55]. After quality control, remaining variants were phased and subsequently imputed onto the reference panel containing the 1000 Genomes Project Phase 3 and around 3,000 Japanese whole-genome sequence data[55]. We restricted subsequent analyses to variants with imputation quality $r^2 > 0.3$. For an association study of age at menopause, we applied a linear mixed model using BOLT-LMM v.2.3.4 software correcting for age in years and the top ten genetically determined principal components as covariates.

The China Kadoorie Biobank baseline survey was conducted during 2004–2008 in ten geographically diverse regions of China (five rural, five urban), with resurveys of approximately 5% of the cohort at 5-yearly intervals. A total of 302,632 women aged 35–74 years were enrolled with a mean age at baseline of 51.4 years (s.d. 10.5), of whom 162,929 provided at least one reported age at menopause, in response to the questions "Have you had your menopause? If so, age of completion of menopause?", with a mean (s.d.) of 48.2 (4.4) years. Genotyping data were available for 31,177 women with values for age at menopause in the range 35–60 years and who had not had prior hysterectomy, oophorectomy, or cancer. Genotyping used custom Affymetrix Axiom arrays with imputation into the 1000 Genomes Phase 3 reference using SHAPEIT3 and IMPUTE4 (IMPUTE2 for chrX). Age at menopause was adjusted for year-of-birth and year-of-birth-squared, and analyses were carried out separately for each of the ten recruitment regions using BOLT-LMM v2.3.2 followed by inverse-variance-weighted fixed effect meta-analysis in METAL. Analyses used CKB data release 15.

The variance explained by our identified signals was estimated using replication summary statistics from a further independent sample of 16,556 women from the Icelandic deCODE study. Of those women, 14,771 were chip-typed and 1,785 were imputed first- and second-degree relatives of chip-typed individuals. We calculated the variance explained by each variant in deCODE (using the formula $2 \times \beta^2 \times \text{MAF} \times (1 - \text{MAF})$), dividing the sum of the variance explained in total for the 290 variants by the s.e.^{2} of menopause age in deCODE.

We additionally estimated the proportion of variance in ANM explained by the 290 genome-wide significant signals in the UK Biobank by calculating linear regression R^2 in 88,829 unrelated women of European descent (as previously described[52]) who had menopause age recorded. We generated estimates by combining the 290 variants as a genetic risk score with the allelic dosage weighted by the effect size from meta-analysis of the 1KG and BCAC strata only (Supplementary Table 2). Genotypes were extracted from imputed data and we included the covariates genotyping chip and release of genotype data, recruitment centre, age and the first five genetic principal components. Genotype-array heritability estimates were calculated using REML implemented in BOLT-LMM to provide a denominator for proportion of heritability explained.

Assessing deviation from an additive genetic model

A dominance deviation test[56] was run for the 290 genome-wide significant ANM signals. In brief, in this test a dominance deviation term representing the heterozygous group (coded 0, 1 and 0) is fitted jointly with an additive genotype term in the regression model. This test determines whether the average trait value carried by the heterozygous group lies halfway between the two homozygote groups as expected under an additive model. We used best guess genotypes converted from UK Biobank imputed genotype data and performed linear regression analysis in Stata v.16.0 in 88,829 unrelated women of European descent (as previously described)[52]. We regressed ANM on genotype including the covariates genotyping chip and release of genotype data, recruitment centre and the first five genetic principal components. We also tested a dominant model, comparing the effect allele heterozygotes/homozygote group with other allele homozygotes, and a recessive model, comparing effect allele homozygotes with heterozygotes and other allele homozygotes. Genetic variants with a P value for the dominance deviation term that was smaller than Bonferonni corrected $P = 0.05$ ($P = 0.05/290 = 0.000172$) were considered to show evidence of non-additive effects.

Gene burden analyses of UK Biobank exome sequencing data

We carried out gene burden association testing of rare variants in women identified from approximately 200,000 people with exome sequencing data available in the UK Biobank study. We included 45,351 women with ANM between 18–65 years in our analyses to maximise the sample size and ensure inclusion of women with POI who might be expected to be more likely to be carriers of rare variants.

Detailed sequencing methodology is provided by ref.[57]. In brief, exomes were captured with the IDT xGen Exome Research Panel v1.0 which targeted 39 Mb of the human genome with coverage exceeding on average 20× on 95.6% of sites. The OQFE protocol was used for mapping and variant calling to the GRCh38 reference. Variants included in our analyses had individual and variant missingness <10%, Hardy–Weinberg equilibrium $P > 10^{-15}$, minimum read depth of 7 for SNPs and 10 for indels, and at least one sample per site passed the allele balance threshold >15% for SNPs and 20% for indels.

Variants in CCDS transcripts were annotated using Variant Effect Predictor[58]. We identified LOF variants (stop-gain, frameshift, or abolishing a canonical splice site (−2 or +2 bp from exon, excluding the ones in the last exon)) deemed to be high confidence by LOFTEE (https://github.com/konradjk/loftee). We conducted gene-burden analyses using a SKAT-O test implemented in SAIGE-GENE[59] based on variants with MAF < 0.001. SAIGE-GENE implements a generalized mixed-model region-based association test that can account for population stratification and sample relatedness in large-scale analyses. We applied an inverse normal rank transformation to ANM before analyses and included recruitment centre as a covariate. For each gene, we present results for the transcript with the smallest SKAT-O P value. Since the magnitude of effect sizes from SAIGE-GENE are not easily interpretable, we calculated the sum of LOF alleles in *BRCA1*, *BRCA2* and *CHEK2* for

each person. We tested each score's association with ANM by performing linear regression in Stata v16.0 in unrelated samples of European descent (identified as previously described[52]) including recruitment centre and the first five genetic principal components as covariates.

Identifying putatively functional genes

We used two in silico approaches to prioritize putatively functional genes across our highlighted loci. First, to identify variants with functional consequences, we looked up variants in $r^2 > 0.8$ with the signals in Variant Effect Predictor (VEP) (build 38). We identified missense, frameshift, insertion/deletions and stop-gained and splice site-disrupting variants, which we then classified according to their VEP, PolyPhen and SIFT impact. We considered 'high impact' variants as those classified as high impact by VEP (stop-gained, frameshift and splice site-disrupting). 'Medium impact' variants were missense variants classed as moderate impact by VEP, which were either deleterious in SIFT or were at least possibly damaging in PolyPhen. 'Low impact' variants were missense or inframe insertions/deletions classed as moderate impact by VEP and were tolerated and/or benign in PolyPhen. LD was calculated using PLINK v.1.9 from best guess genotypes for 1000 Genomes Phase 3/HRC imputed variants in approximately 340,000 unrelated UK Biobank participants of white British ancestry. Genetic variant locations were converted from b37 to b38 using UCSC Liftover.

Second, we integrated our ANM genome-wide summary statistics with eQTL data using summary Mendelian randomization (SMR)[60]. Publicly available expression datasets for 48 tissues in GTEx v.7 and 10 brain regions were downloaded from the SMR website (https://cnsgenomics.com/software/smr/#eQTLsummarydata). Whole-blood data in an eQTL meta-analysis of 31,684 samples was available from the eQTLGen consortium[61]. A Bonferroni corrected P value threshold was used in each expression dataset individually and only associations with HEIDI $P > 0.01$ were considered to avoid coincidental overlap due to extended patterns of LD. This resulted in a total of 44 (SMR $P < 7 \times 10^{-6}$) significant transcriptions in the brain, 96 in whole blood ($P < 3 \times 10^{-6}$) and 732 across all GTEx tissues (SMR $P < 3.6 \times 10^{-7}$). We excluded brain and whole blood tissues from the collection of 48 tissues in GTEx as they were better represented by the other expression datasets.

Identifying enriched cell and tissue types

We used three approaches to identify cell and tissue types enriched for ANM-associated variants. DEPICT was run using default settings as previously described[62] using GWAS summary statistics including all autosomal variants with $P < 1 \times 10^{-5}$. The cell-type-specific expression matrices used as input to DEPICT were generated from individual single-cell gene expression datasets (see below). In brief, each dataset was processed by first normalizing cells's gene expression to a common transcript count (10,000 transcripts per cell) before calculating the average expression of each gene for each cell-type annotation. Averaged data were log-transformed (natural log). We computed cell-type-specific gene expression using a two-step z-score approach. First, we calculated gene-wise z-scores (each gene; mean = 0, s.d. = 1) to remove the effect of ubiquitously expressed genes, and then we calculated cell-type-wise z-scores (each cell-type; mean = 0, s.d. = 1) on gene-wise z-scores. For mouse expression datasets, we mapped mouse genes to human orthologues using Ensembl (v. 91) keeping only genes with a 1–1 orthologue mapping.

DEPICT analyses were run on two datasets. (1) Tabula Muris (https://tabula-muris.ds.czbiohub.org/)[63], restricted to the fluorescence-activated cell sorting samples. To keep the tissue-level information in the dataset, we defined cell-type annotations as 'tissue cell-types' by combining the cell-type label ('cell_ontology_class' column) with the origin tissue of the cell-type ('tissue' column). This allowed us to, for example, distinguish among B cells originating from fat, spleen and marrow tissue. In total, we analysed 115 cell-type annotations from 44,949 cells. (2) The published human haematopoietic stem and progenitor cell differentiation dataset[64] was not normalized to a common transcript count because the data were pre-normalized by the authors. We defined cell-type annotations as the 12 distinct haematopoietic stem and progenitor cell (HSPC) phenotypes reported by the authors (shown in figure 3a of their paper). The annotations covered 1,483 cells.

Second, we additionally performed tissue enrichment analysis using LD score regression to specifically expressed genes (LDSC-SEG)[65]. We used three datasets available on the LDSC-SEG resource page (https://github.com/bulik/ldsc/wiki/Cell-type-specific-analyses), relating to cell and tissue-specific annotations from GTEx[66], Epigenome Roadmap[67] and the Franke laboratory[62,68].

Finally, tissue enrichment analyses were performed using 'Downstreamer', which is described in a separate section below.

Pathway analysis

MAGENTA was used to explore pathway-based associations in the full GWAS dataset. MAGENTA implements a gene set enrichment analysis (GSEA)-based approach[69]. We used upstream and downstream limits of 110 kb and 40 kb, respectively, to assign variants to genes, excluded the HLA region from the analysis and set the number of permutations to 10,000 for GSEA testing, with analysis using 75% and 95% cut-offs. Significance was determined when an individual pathway reached a false discovery rate (FDR) < 0.05 in either analysis. In total, 3,222 pathways from Gene Ontology, PANTHER, KEGG and Ingenuity were tested for enrichment of multiple modest associations with ANM.

We also performed pathway analyses in 'Downstreamer' (described below) and MAGMA[70] v1.08. MAGMA analyses were performed using the full genome-wide summary statistics, but restricted to variants that were predicted as deleterious (that is, non-synonymous and LOF). Gene sets included in the analyses were obtained from MsigDB v7.2, which included 12,358 curated gene sets from KEGG, Reactome, BioCarta and GO terms consisting of biological processes, cellular components and molecular functions.

Downstreamer methodology

In short, Downstreamer identifies genes connected to genes at GWAS loci (core genes) through expression and identifies enriched pathways. Downstreamer implements a strategy that accounts for LD structure and chromosomal organization, operating in two steps. In the first step, gene-level prioritization scores are calculated for the GWAS trait and a null distribution. In the second step, the gene-level prioritization scores are associated with the co-regulation matrix and pathway annotations. Further details are outlined below.

Downstreamer step 1

Calculation of gene-level prioritization scores (GWAS gene z-scores). The primary step is to convert GWAS summary statistics from P values per variant to an aggregate P value per gene (gene P value) while accounting for local LD structure. This aggregate gene level P value represents the GWAS signal potentially attributable to that gene.

First, we applied genomic control to correct for inflation in the GWAS signal. We then integrated the procedure from the PASCAL[71] method into Downstreamer to aggregate variant P values into a gene P value while accounting for the LD structure. We aggregated all variants within a 25-kb window around the start and end of a gene using the non-Finnish European samples of the 1000 Genomes (1000G) project, Phase 3 to calculate LD. We calculated these GWAS gene P values for all 20,327 protein-coding genes (Ensembl release v.75). The gene P values were then converted to z-scores for use in subsequent analysis. These are referred to as GWAS gene z-scores.

Calculation of gene z-scores for null GWASs to account for chromosomal organization of genes and to calculate empirical P values. To account for long-range effects of haplotype structure, which results in genes getting a similar GWAS gene z-score, we use a generalized

least-squares (GLS) regression model for all regressions done in Downstreamer. The GLS model takes a correlation matrix that models this gene–gene correlation.

To calculate this correlation matrix we first simulated 10,000 random phenotypes by drawing phenotypes from a normal distribution and then associating them to the genotypes of the 1000G Phase 3 non-Finnish European samples. We used only overlapping variants between the real traits and the permuted GWASs to avoid biases introduced by genotyping platforms or imputation. We then calculated the GWAS gene *z*-scores for each of the 10,000 simulated GWAS signals as described above. Next, we calculated the Pearson correlations between the GWAS gene *z*-scores. As simulated GWAS signals are random and independent of each other, any remaining correlation between GWAS gene *z*-scores reflects the underlying LD patterns and chromosomal organization of genes.

We simulated an additional 10,000 GWASs as described above to empirically determine enrichment *P* values and, finally, we used an additional 100 simulations to estimate the FDR of Downstreamer associations.

Downstreamer step 2

Calculation of *z*-scores for co-regulation matrix. To calculate core scores, we used a previously generated co-regulation matrix that is based on a large multi-tissue gene network[72]. In short, publicly available RNA-seq samples were downloaded from the European Nucleotide Archive (https://www.ebi.ac.uk/ena). After QC, 56,435 genes and 31,499 samples covering a wide range of human cell-types and tissues remained. We performed a PCA on this dataset and selected 165 components representing 50% of the variation that offered the best prediction of gene function. We then selected the protein-coding genes and centred and scaled the eigenvectors for these 165 components (mean = 0, s.d. = 1) such that each component was given equal weight. The first components mostly describe tissue differences[72], so this normalization ensures that tissue-specific-patterns do not disproportionately drive the co-regulation matrix. The co-regulation matrix is defined as the Pearson correlation between the genes from the scaled eigenvector matrix. The diagonal of the co-regulation matrix was set to zero to avoid the correlation with itself having a disproportionate effect on the association to the GWAS gene *z*-scores. Finally, we converted the Pearson *r* to *z*-scores.

Calculation of *z*-scores for pathways and gene sets. To identify pathway and disease enrichments, we used the following databases: Human Phenotype Ontology (HPO), Kyoto Encyclopaedia of Genes and Genomes (KEGG), Reactome and Gene Ontology (GO) Biological Process, Cellular Component and Molecular Function. We have previously predicted how much each gene contributes to these gene sets, resulting in a *z*-score per pathway or term per gene[72]. We collapsed genes into meta-genes in parallel with the GWAS step, to ensure compatibility with the GWAS gene *z*-score following the same procedure as in the GWAS pre-processing. Meta-gene *z*-scores were calculated as the *z*-score sum divided by the square root of the number of genes. Finally, all pathway *z*-scores were scaled (mean = 0, s.d. = 1).

Pre-processing of GWAS gene *z*-scores and pruning of highly correlated genes. For each GWAS, both real and simulated, we carried out rank-based inverse normal transformation of GWAS *z*-scores to ensure that outliers would not have disproportionate weights. Owing to limitations in the PASCAL methodology that result in ties at a minimum significance level of 1×10^{-12} for highly significant genes, we used the minimum SNP *P* value from the GWAS to identify the most significant gene and resolve the tie. We then used a linear model to correct for gene length, as longer genes will typically contain more SNPs.

Sometimes, two (or more) genes will be so close to one another that their GWAS gene *z*-scores are highly correlated, violating the assumptions of the linear model. Thus, genes with a Pearson correlation $r \geq 0.8$ in the 10,000 GWAS permutations were collapsed into 'meta-genes' and treated as one gene. Meta-gene *z*-scores were averaged across the input *z*-scores. Lastly, the GWAS *z*-scores of the meta-genes were scaled (mean = 0, s.d. = 1).

GLS model to calculate pathway enrichment and core gene scores

We used a GLS regression to associate the GWAS gene *z*-scores to the pathway *z*-scores and co-regulation *z*-scores (described below). These two analyses result in the pathway enrichments and core gene prioritizations, respectively. We used the gene–gene correlation matrix derived from the 10,000 permutations as a measure of conditional covariance of the error term (Ω) in the GLS to account for the relationships between genes due to LD and proximity. The pseudo-inverse of Ω is used as a substitute for Ω^{-1}.

The formula of the GLS is $\beta = (X^T\Omega^{-1}X)^{-1}X^T\Omega^{-1}\mathbf{y}$, where β is the estimated effect size of a pathway, term or gene from the co-regulation matrix, Ω is the gene–gene correlation matrix, X is the design matrix of real GWAS *z*-scores and $\mathbf{y}$ is the vector of gene *z*-scores per pathway, term or gene from the co-regulation matrix. As we standardized the predictors, we did not include an intercept in the design matrix and X contains only one column with the real GWAS gene *z*-scores. We estimated the βs for the 10,000 random GWASs in the same way and subsequently used them to estimate the empirical *P* value for β.

Definition of POI and DDR genes

We combined genes implicated in the DDR from a number of sources yielding a total of 778 genes[73–75] (Supplementary Table 19). To identify genes associated with premature ovarian insufficiency/primary ovarian insufficiency (ICD-11 GA30.6), we carried out a search in PubMed for premature ovarian insufficiency, primary ovarian insufficiency, premature ovarian failure and ovarian dysfunction in humans and reviewed all primary studies published in English up to 22 July 2020. We included syndromic, non-syndromic, sporadic and familial single-nucleotide variants, insertion/deletions and copy number variants (CNVs) and included 114 genetic variants from 139 studies. We did not attempt to review the clinical significance of the variants, which ranged from classical POI genes to newly identified CNVs in whole-exome sequencing studies. We expanded our search to review articles and ClinVar. We uncovered another four genes implicated in Perrault syndrome for which our search terms were not included in the original articles. This gave a total of 118 genes. Our search detected all genetic variants entered in ClinVar as pathogenic, likely pathogenic or with conflicting interpretations of pathogenicity. We excluded genes with variants when no assertion criteria were provided and no published data were available for assessment in ClinVar. Two studies of large chromosomal rearrangements as well as quantitative trait loci consisting of more than a single genetic variant from GWAS in POI populations were excluded, resulting in 74 genes (Supplementary Table 6). Gene lists were curated independently of the current meta-analysis and genes were included only if there was convincing evidence independent of any GWAS study.

Polygenic prediction of early menopause

To evaluate the effect of common variants on clinical extremes of ANM, we first performed a GWAS meta-analysis excluding the UK Biobank study (n = 95,275). Effect estimates from this analysis (Supplementary Table 2) were then used for subsequent polygenic score (PGS) construction of ~6.97 million autosomal variants across the genome using LDPRED[76]. The PGS was calculated using PLINK[77] v.1.90b4.4 in an independent sample of 108,840 women with the full phenotypic range of ANM ages from the UK Biobank study, rescaled to have a mean of 0 and s.d. of 1. We then estimated the centile distribution of the genetic risk score for all women with a valid ANM (with no lower or upper phenotype boundary). Two outcomes were defined: early menopause (EM)

defined as ANM < 45 (n = 11,268) versus all other women (n = 97,572); and premature ovarian insufficiency (POI), defined as ANM < 40 years (n = 2,407) versus all other women (n = 106,433). Logistic regression analyses, adjusting for age, genotype array and ten genetic principal components, were then performed with either EM or POI as the outcome. This was performed 99 times for each centile of genetic risk (coded 1) versus the 50th centile of genetic risk (coded 0). To assess the relevance of this score to each ANM age group, we estimated the average PGS value by year of ANM. For example, we grouped all women with ANM = 47 and estimated the mean and s.e. of the PGS in this group of women. Our intuition was that any ANM range not influenced by common genetic variants would have the population mean PGS (that is, mean = 0 and s.d. = 1). Receiver operating characteristics (ROC) models were performed in Stata v.14 using the roctab, rocgold and rocreg commands.

Mendelian randomization analyses

To infer causal relationships between ANM and other health related outcomes, we performed Mendelian randomization (MR). The 290 independent ANM signals were used as a genetic instrument for later ANM. Where a signal was not present in the outcome GWAS, we identified the best HapMap2 proxy with $r^2 > 0.5$ within 250 kb either side of the signal and its relevant weight was included in our genetic instrument (Supplementary Table 23). The genetic variants were identified in publicly available GWAS datasets for a range of outcomes of interest (Supplementary Table 22). These were used in three methods of MR: inverse variance weighted[78], MR-EGGER[79] and weighted median[80]. As a sensitivity analysis we additionally removed signals that appeared to be outliers. This was achieved using the Radial method considering the IVW model[81]. We also performed MR considering the effect of a range of putative modifiable risk factors on ANM as the outcome using the same MR models. Genetic instruments were created for the risk factors using independent genetic variants with effects estimated in published GWAS (Supplementary Table 25). For the risk factors of cigarette exposure and alcohol consumption, the MR was performed with a single genetic variant by calculating a Wald ratio for the effect of the variants on ANM divided by the effect on the risk factor using mrrobust in Stata v.16.0. The effect of the genetic variant for alcohol consumption was measured in log(drinks per week) (note that 'drink' is a US measure of alcohol consumption equal to 14 g pure alcohol, equivalent to 1.75 UK units). Hence a change from 1 drink to 7 drinks (US maximum recommended per week) would be the equivalent of a 1.95 increase in log(drinks per week), which when applied to the Wald estimate, gives the respective change in age at menopause.

Expression of candidate genes identified by human GWAS in a mouse model of environmentally induced low ovarian reserve

Generation of mouse model. All animal experiments underwent ethical review by the University of Cambridge Animal Welfare and Ethical Review Board and were carried out under the UK Home Office Animals (Scientific Procedures) Act (1986, United Kingdom). Female C57BL/6J mice were randomized to be fed ad libitum either a standard laboratory chow diet (7% simple sugars/3% fat; Special Dietary Services) or an obesogenic diet (10% simple sugars/20% animal lard; Special Diets Services). The obesogenic diet was supplemented with a separate pot of sweetened condensed milk (55% simple sugars/8% fat; Nestle UK) available to the mice within the cage. A detailed description of the dietary regimen has previously been published[82]. Female mice were placed on the allocated diet six weeks before first mating with wild-type males on standard chow diet. The first litter was discarded after weaning, and only proven-breeder females were used for the experimental protocols. Second matings occurred once females on the obesogenic diet had reached at least 10 g absolute fat mass, as assessed by time domain nuclear resonance imaging (TDNMR) (Minispec Time Domain Nuclear Resonance, Bruker Optics). The female mice remained on their allocated diets throughout the breeding, pregnancy, and lactation phases. After delivery, each litter was culled to six pups at random to standardize their plane of nutrition from postnatal day 3 in all litters. There was no significant difference in the pre-culling litter size between obesogenic and control litters. Equal sex ratios within the litters were maintained as far as possible. After weaning at day 21, female offspring were randomly allocated to either the control or the obesogenic diets (identical to those used for the dams) and remained on these diets for the duration of the study. Bodyweight and food intake were measured weekly. At 12 weeks of age, offspring total and fat mass were assessed by weighing and by TDNMR (Minispec Time Domain Nuclear Resonance, Bruker Optics), respectively. Following an overnight fast, the female offspring were weighed and then culled by CO_2 asphyxiation and cervical dislocation. Ovaries were dissected and weighed immediately. One ovary from each mouse was snap-frozen in liquid nitrogen or dry ice, and stored at −80 °C, and the other was fixed in formalin/paraldehyde. The fixed ovary was sectioned and subjected to haematoxylin and eosin (H&E) staining to ensure equal distribution of oestrous stages in each experimental group (data not shown). Detailed reproductive and metabolic phenotyping of the female pups has previously been published[24].

Gene expression analysis. A screen of 35 DDR genes highlighted by a previous GWAS on ANM were selected for investigation[13]: *Brca1*, *Bre*, *Brsk1*, *Chd7*, *Chek2*, *Dido1*, *Fbxo18*, *Helb*, *Helq*, *Mcm8*, *Mlf1ip*, *Msh5*, *Msh6*, *Mycbp*, *Polg*, *Prim1*, *Rad51*, *Rad54l*, *Rev3l*, *Uimc1*, *Apex*, *Aptx1*, *Cdk2ap1*, *Dmc1*, *Exo1*, *Fam175a*, *Fanci*, *Ino80*, *Kntc1*, *Papd7*, *Parl*, *Parp2*, *Polr2e*, *Polr2h* and *Tlk1*. Expression levels were measured in whole snap-frozen ovaries. RNA was extracted using a miRNeasy mini Kit (Qiagen). The kit was used according to the manufacturer's instructions, with the addition of DNaseI digestion to ensure that the samples were free from genomic DNA contamination. The extracted RNA was quantified using a Nanodrop spectrophotometer (Nanodrop Technologies). cDNA was synthesized from 1 µg RNA using oligo-dT primers and M-MLV reverse transcriptase. Gene expression was quantified via RT–PCR (StepOne Plus machine; Applied Biosystems) using custom-designed primers (Sigma) and SYBR green reagents (Applied Biosystems). Equal efficiency of reverse transcription between all groups was confirmed using the housekeeper gene *Ppia*, and absence of gDNA contamination was confirmed by quantifying *Myh6*, which was absent in all samples.

Statistical analysis. All data were initially analysed using a two-way ANOVA with maternal diet and offspring diet as the independent variables. In order to correct for multiple hypothesis testing of gene expression levels, P values were transformed to q values to take account of the FDRs using the p.adjust function in R stats package (R Foundation for Statistical Computing). Data are represented as mean ± s.e.m. Where P values are reported, an alpha level <0.05 was considered statistically significant. All data analysis was conducted using the R statistical software package version 2.14.1 (R Foundation for Statistical Computing). In all cases, n refers to the number of litters, and n = 8 for all groups. Study power was determined on the basis of effect sizes for gene expression differences observed in our previous studies of this model[24].

Human oocytes mRNA screen

Research on RNA expression in human eggs was carried out according to the Helsinki II declaration and was conducted in accordance with national regulation on research on human subjects and material. The research was approved by the Scientific Ethical Committee of the Capital Region of Denmark (Videnskabsetisk Komite) in accordance with Danish National regulation (H-2-2011-044; extension licence amm. nr. 51307; licence holder: C.Y.A. and H-1604473; licence holder: E.R.H.; H-16027088 granted to M.L.G.). The full protocols contained permission to conduct mRNA sequencing on human eggs. GDPR approval

was obtained from the national data agency (SUND-2016-60, E.R.H. and HGH-2016_086 to M.L.G.). All participants provided informed consent according to Danish ethical regulations after receiving written information and oral clarification about participation. Participants could withdraw from the study at any time. Participants did not receive monetary compensation and their participation was fully voluntary and did not affect their fertility treatment.

Single human MII oocytes were collected as previously described[83], lysed in-tube and the cDNA was amplified according to the manufacturer's instructions (Takara Bio; mRNA-Seq, SMART-Seq v4 ultra low input RNA kit, cat. no. 634894). The quality of individual cDNA libraries was verified on an Agilent 2100 Bioanalyzer instrument using a high-sensitivity DNA kit (Agilent, 5067-4626). The libraries were prepared with 100 pg input using the Nextera XT DNA library preparation kit (Illumina, FC-131-1024) and the Nextera XT index kit v2 (FC-131-2002) and quantified on a Qubit 3.0 fluorimeter (Thermo Fisher Scientific, Q32854). The quality of the final library was verified on the Agilent 2100 Bioanalyzer high-sensitivity DNA chip and pooled to 4 nM. The 4 nM library pools were denatured and loaded according to the recommended NextSeq500 guidelines (Illumina).

Expression analysis of GWAS genes in human oocytes and granulosa cells at various stages of development. We used processed RNA-seq data from fetal primordial germ cells (Gene Expression Omnibus (GEO) accession code: GSE86146)[84] from 17 human female embryos ranging from 5 to 26 weeks post-fertilisation, and from follicles at 5 different stages of development from fresh ovarian tissue from 7 adult donors, separated into oocytes and granulosa cell fractions (GEO accession code GSE107746)[85]; in addition to our MII oocytes single-cell RNA-seq dataset (described below).

We transformed the per-cycle base call (BCL) file output from the sequencing run of 11 human MII oocytes into per-read FASTQ files using the bcl2fastq2 Conversion Software v.2.19 from Illumina. The sample libraries were multiplexed across four sequencing lanes and the FastQ files from each of the four lanes were concatenated to generate one set of paired fastq files per sample. We performed sample QC and filtering of reads to remove low-quality reads, adaptor sequences and low-quality bases with trimmomatic[86] version 0.36 in two steps using ILLUMINACLIP:/ /Trimmomatic-0.36/adapters/NexteraPE-PE.fa:2:30:10 (SLIDINGWINDOW:4:20 CROP:72 HEADCROP:10 MINLEN:40 followed by an extra trim of headbases with HEADCROP:10.) Subsequent to filtering, we used the remaining paired reads for alignment by hisat2[87] to the human genome GeneCode v.27 release with the paired GenCode v.27 gtf file containing gene annotations using: ($HISAT2 -p 22 --dta -x .gencode.v27 -1 R1.fastq -2 R2.fastq -S sample.sam)[88]. The resulting .sam files were sorted, indexed and transformed to .bam files using samtools[89]. QC measures of aligned reads was generated using picard metrics (https://slowkow.github.io/picardmetrics) and the CollectRnaSeqMetrics tool from picard tools (http://broadinstitute.github.io/picard). We filtered the bam files for mitochondrial reads and Stringtie was applied to merge and assemble reference-guided transcripts for gene level quantifications of raw counts, and transcripts per million (TPM)[88]. Of the 283 consensus genes highlighted by the GWAS (Supplementary Table 5), 258 passed QC and were available in the expression dataset. Gene expression levels in TPM were used for further analyses as this unit allows efficient comparison of gene expression levels between samples from different studies. A pseudo-count of 1 was added to all TPM values and converted to $\log_2$ scale before the heat maps were plotted. Hierarchical clustering by euclidean distance, *z*-score calculation and plotting the heat map was done using the R package 'pheatmap' v. 1.0.12 (https://cran.r-project.org/web/packages/pheatmap/pheatmap.pdf). *z*-scores were calculated by subtracting the mean of TPM values in all samples for a gene and dividing by the s.d. Only samples with TPM > 5 were considered for the heat map showing the GWAS genes.

***sChek1*, *Chek1* conditional knockout (cKO), and *Chek2* mice**

Mouse work at the University of Copenhagen (*sChek1*) was licensed under 2016-15-0202-00043 by the Danish Animal Experiments Inspectorate (Dyreforsøgstilsynet, Denmark). Mouse work at UAB (Chek2) was approved by the UAB and the Catalan Ethics Committee for Animal Experimentation (CEEAAH 1091; DAAM6395). Mouse work at CCHMC (*Chek1* cKO, *Ddx4-Cre*) was performed according to the guidelines of the Institutional Animal Care and Use Committee (protocol no. IACUC2018-0040) and approved by CCHMC. The *Chek1* cKO, *Zp3-Cre* embryology was conducted at the Institute of Animal Physiology and Genetics CAS in Libechov (Czech Republic), abiding by the policies of the Expert Committee for the Approval of Projects of Experiments on Animals of the Academy of Sciences of the Czech Republic (no. 43-2015).

Chek1 cKO (*Ddx4-Cre*), *sChek1* and *Chek2* mutant mice were previously generated[36,40,90]. The lines were maintained in C57BL/6-129Sv and inbred C57BL/6-129Sv (*sChek1* and *Chek2*) backgrounds, respectively. The *Chek2* mouse is available under accession number BRC03481 at the RIKEN Bioresource Centre. The *Chek1* cKO *Zp3-Cre* embryos were generated by crossing mice with the *Zp3-Cre* transgene[91] to mice with a *Chek1* allele containing *LoxP* sites[92] resulting in mice expressing Cre-recombinase under the control of the oocyte-specific *Zp3* promotor (*Zp3::Cre*) to produce *Chek1* cKO (*Zp3-Cre*). All experiments were carried out using littermate controls or with mice of closely related parents as controls. The four mutant strains were kept at the University of Copenhagen (*sChek1*), Autonomous University of Barcelona (*Chek2*), Cincinnati Children's Hospital Medical Center (*Chek1* cKO (*Ddx4-Cre*)) and Institute of Animal Physiology and Genetics CAS in Libechov, Czech Republic (*Chek1* cKO *Zp3-Cre*). Breeding cages were set up in a conventional way with a strict specific pathogen-free barrier and mice used for experiments were kept in individual ventilated cages (IVCs). Twelve-hour light exposure was provided. Temperature, relative humidity and air changes per hour were 22 °C (±2 °C), 55% ± 10%, and 17 respectively. Food and water were provided ad libitum. Mice were genotyped twice, initially upon weaning and again before experimental procedures were carried out. Mouse genotyping was performed by PCR analysis using the following primers for the *Chek1* cKO *(Ddx4)*: F1

Mouse ovarian histology and follicle count. Ovaries were dissected and placed in 4% formaldehyde (*Chek1* cKO (*Ddx4*)) and Bouin's fixative solution (70% saturated picric acid solution (Applichem, A2520, 1000), 25% formaldehyde, 5% glacial acetic acid (Merck, 1.00063.2500)) overnight at 4 °C. The ovaries were washed twice with cold PBS for 30 min followed by dehydration with an increasing concentration of ethanol. Subsequently, the samples were submerged in Histo-Clear II (Cat. No. HS-202, National Diagnostics) for 30 min. at room temperature. This was repeated another two times (three times in total) with fresh Histo-Clear II. Ovaries were embedded in paraffin blocks and cut to a thickness of 7 µm (*sChek1* and *Chek2)* and 6 µm (*Chek1* cKO (*Ddx4-Cre*)) and mounted on poly-L-lysine-coated slides. After de-paraffinization and rehydration, the slides were stained with PAS-haematoxylin. The tissue was imaged using a Zeiss Axio scanner Z.1 and follicles with a visible nucleus were counted using Zen Blue lite software from Zeiss. Primordial follicles contain one layer of flat granulosa cells surrounding the oocytes, and primary follicles have one layer of cuboid granulosa cells. Secondary follicles contain two or more layers of granulosa cells, and antral follicles are those with one or several cavities (the antrum).

Mouse ovulation induction and oocyte collection. Ovulation was induced by injection of 7.5 IU of PMSG (Prospec; ref HOR-272) followed by 7.5 IU of hCG (Chorulon Vet; ref 422741) after 47 h. Twelve hours after the hCG injection, the mice were killed and oviducts were dissected under a stereo-microscope to release the cumulus masses into 90-µl drops of fertilization medium covered with mineral oil (NordilCell; ref 90142). Oocytes were recovered from oviducts by gently tearing the

swollen ampullae of oviducts to release cumulus masses into medium. The recipe for fertilization medium was previously published[93].

RT–qPCR on mice oocytes. Total RNA from oocytes was isolated with the Arcturus PicoPure RNA Isolation Kit from Applied Biosystems following the manufacturer's instructions. Reverse transcription reactions were done with 28 ng RNA using the Maxima First Strand cDNA Synthesis Kit for RT–qPCR with dsDNase (Thermo Fisher Scientific). cDNA was quantified by qPCR with the Applied Biosystems 7500 FAST Real-Time PCR System using Power SYBR green PCR Master Mix from Thermo Fisher Scientific. The sequences of the primers used are the following: *Chek1*-For:.

Mouse embryo development in vitro. Fresh pre-thawed frozen sperm from a proven fertile C57BL/6 wild-type male was used for in vitro fertilization and poured into a dish containing mature MII eggs in fertilization medium. Disappearance of the germinal vesicle (GV) and polar body extrusion confirmed fertilization. Zygotes were incubated with 5% CO_2 at 37 °C. After incubating zygotes in fertilization medium overnight, we transferred zygotes to a 60-mm Petri dish containing 50 µl KSOM (Chemicon, cat MR-106-D) covered by mineral oil (NordilCell; ref 90142). Two separate dishes were prepared for embryos from each genotype. The embryos were again incubated with 5% CO_2 at 37 °C. The developmental stage of embryos was assessed using a stereomicroscope at the equivalent of 0.5, 1.5, 2.5, 3.5, 4.4 and 5.5 days post-coitum (dpc). For *chek2*, where the wild-type frequency of fertilization was lower than in the *Chek1*-cko and *sChek1* strains, we used young C57BL/6J. Ola.Hsd females to control for the efficiency of IVF (85%).

Mouse ovulation and embryo development (*Chek1* cKO, *Zp3-Cre*). *Chek1* control and cKO females were stimulated with 5 IU of PMSG (HOR-272, Prospec) followed by 5 IU of hCG (Ovitrelle, Merck) after 44 h. After 18 h, the females were killed using cervical dislocation according to the protocols authorized by the ethics committee, and ovulated MII oocytes and zygotes were collected in M2 medium (M7167-50ML, Sigma-Aldrich) by tearing ampullae from oviducts. The oocytes and zygotes in the cumulus mass were placed into a drop of M2 medium supplied with 300 µg/ml hyaluronidase (H4272, Sigma-Aldrich) to release the cumulus cells. The MII oocytes and zygotes were cultured with 5% CO_2 at 37 °C in EmbryoMax KSOM medium (MR-106-D, Sigma-Aldrich) and after 10 h were scored using a Leica DMI 6000 microscope. Only zygotes with visible pronuclei were left for subsequent culture.

Immunofluorescence analysis of mouse preimplantation embryos (*Chek1* cKO, *Zp3-Cre*). The embryos were briefly washed three times in PBS supplied with 1 mg/ml poly(vinyl alcohol) and fixed in 3.7% formaldehyde for 45 min. They were permeabilized thereafter by 0.5% Triton X-100 in PBS for 45 min. To block nonspecific antibody binding, the embryos were incubated in 2% normal donkey serum (NDS) for 2 h. The embryos were incubated overnight at 4 °C with primary antibody against gH2AX at a dilution of 1:200 (9718, Cell Signaling Technology). The next day, they were incubated for 90 min at a dilution 1:100 in rhodamine (TRITC)-AffiniPure Donkey Anti-Rabbit IgG (711-025-152, Jackson Immuno Research). Then they were mounted in ProLong Gold Antifade Mountant with DAPI (P36941, Invitrogen) with a spacer to uphold the 3D embryonic structure. The embryos were washed five times for 8 min in PBS supplied with 1 mg/ml bovine serum albumin or 0.2% NDS between each step. The embryos were scanned using a confocal microscope (Leica TCS SP5) and Fiji software[94] was used for image analysis.

Mouse embryo transfer. Wild-type female recipient mice (surrogates) were prepared to receive embryos by mating them with an infertile male one night before the transfer of embryos. Successful preparation of recipient mice for embryo transfer was confirmed by checking for the presence of a plug. Two cell-stage (1.5 dpc) embryos were transferred into a single horn of recipient mice and anaesthesia was maintained during this procedure. Pups were born 19 days after embryo transfer.

Natural breeding, assessment of health of offspring and fertility in mouse. To test the natural breeding efficiency, we set cages with one or two adult (2- or 12-month-old) control female mice with a male of proven fertility. We registered litter sizes and dates of delivery for all litters obtained during a period of up to one year.

Mice serum AMH analysis. Mice of various ages were anaesthetized. Blood was collected in a plain tube, allowed to clot for one hour at room temperature and then centrifuged at 3,000 rpm (1,500*g*) for 15 min at 4 °C. After centrifugation, supernatant (serum) was collected in a 1.5-ml tube and stored at −80 °C. Serum AMH levels were determined using an AMH ELISA kit (cat. no. AL-113) from Ansh Labs.

Assessment of the health of offspring from control and mutant breeding was performed on a weekly basis by the personnel of the respective animal facilities following the standard health monitoring protocols approved by the Copenhagen or Catalan Ethics Committee for Animal Experimentation.

Reporting summary

Further information on research design is available in the Nature Research Reporting Summary linked to this paper.

Data availability

Full genome-wide association summary statistics for the discovery meta-analysis are available from the ReproGen website (www.reprogen.org). The MII oocyte dataset is available from the European Genome-Phenome Archive under accession EGAS00001004947 (https://ega-archive.org/studies/EGAS00001004947). Access to these data is granted in accordance with the ethics permissions under which the data were collected from participants and under appropriate GDPR compliant data processing agreements. Data from the following sites were used: SMR (https://cnsgenomics.com/software/smr/#eQTLsummarydata); Tabula Muris (https://tabula-muris.ds.czbiohub.org/); LDSC-SEG (https://github.com/bulik/ldsc/wiki/Cell-type-specific-analyses); RNA-seq samples (https://www.ebi.ac.uk/ena); human oocyte expression analyses: Gene Expression Omnibus GSE86146, GSE107746. Source data are provided with this paper.

51. Bycroft, C. et al. The UK Biobank resource with deep phenotyping and genomic data. *Nature* **562**, 203–209 (2018).
52. Tyrrell, J. et al. Using genetics to understand the causal influence of higher BMI on depression. *Int. J. Epidemiol.* **48**, 834–848 (2019).
53. Loh, P.-R. et al. Efficient Bayesian mixed-model analysis increases association power in large cohorts. *Nat. Genet.* **47**, 284–290 (2015).
54. Yang, J., Lee, S. H., Goddard, M. E. & Visscher, P. M. GCTA: a tool for genome-wide complex trait analysis. *Am. J. Hum. Genet.* **88**, 76–82 (2011).
55. Terao, C. et al. Chromosomal alterations among age-related haematopoietic clones in Japan. *Nature* **584**, 130–135 (2020).
56. Wood, A. R. et al. Variants in the FTO and CDKAL1 loci have recessive effects on risk of obesity and type 2 diabetes, respectively. *Diabetologia* **59**, 1214–1221 (2016).
57. Szustakowski, J. D. et al. Advancing human genetics research and drug discovery through exome sequencing of the UK Biobank. *Nat. Genet.* https://doi.org/10.1038/s41588-021-00885-0 (2021).
58. McLaren, W. et al. The Ensembl variant effect predictor. *Genome Biol.* **17**, 122 (2016).
59. Zhou, W. et al. Scalable generalized linear mixed model for region-based association tests in large biobanks and cohorts. *Nat. Genet.* **52**, 634–639 (2020).
60. Zhu, Z. et al. Integration of summary data from GWAS and eQTL studies predicts complex trait gene targets. *Nat. Genet.* **48**, 481–487 (2016).
61. Võsa, U. et al. Unraveling the polygenic architecture of complex traits using blood eQTL metaanalysis. Preprint at https://doi.org/10.1101/447367 (2018).
62. Pers, T. H. et al. Biological interpretation of genome-wide association studies using predicted gene functions. *Nat. Commun.* **6**, 5890 (2015).
63. Tabula Muris Consortium. Single-cell transcriptomics of 20 mouse organs creates a Tabula Muris. *Nature* **562**, 367–372 (2018).
64. Nestorowa, S. et al. A single-cell resolution map of mouse hematopoietic stem and progenitor cell differentiation. *Blood* **128**, e20–e31 (2016).
65. Finucane, H. K. et al. Heritability enrichment of specifically expressed genes identifies disease-relevant tissues and cell types. *Nat. Genet.* **50**, 621–629 (2018).

66. GTEx Consortium. The Genotype-Tissue Expression (GTEx) pilot analysis: multitissue gene regulation in humans. *Science* **348**, 648–660 (2015).
67. Roadmap Epigenomics Consortium et al. Integrative analysis of 111 reference human epigenomes. *Nature* **518**, 317–330 (2015).
68. Fehrmann, R. S. N. et al. Gene expression analysis identifies global gene dosage sensitivity in cancer. *Nat. Genet*. **47**, 115–125 (2015).
69. Segrè, A. V., Groop, L., Mootha, V. K., Daly, M. J. & Altshuler, D. Common inherited variation in mitochondrial genes is not enriched for associations with type 2 diabetes or related glycemic traits. *PLoS Genet*. **6**, e1001058 (2010).
70. de Leeuw, C. A., Mooij, J. M., Heskes, T. & Posthuma, D. MAGMA: generalized gene-set analysis of GWAS data. *PLoS Comput. Biol*. **11**, e1004219 (2015).
71. Lamparter, D., Marbach, D., Rueedi, R., Kutalik, Z. & Bergmann, S. Fast and rigorous computation of gene and pathway scores from SNP-based summary statistics. *PLoS Comput. Biol*. **12**, e1004714 (2016).
72. Deelen, P. et al. Improving the diagnostic yield of exome- sequencing by predicting gene-phenotype associations using large-scale gene expression analysis. *Nat. Commun*. **10**, 2837 (2019).
73. Knijnenburg, T. A. et al. Genomic and molecular landscape of DNA damage repair deficiency across The Cancer Genome Atlas. *Cell Rep*. **23**, 239–254.e6 (2018).
74. Pearl, L. H., Schierz, A. C., Ward, S. E., Al-Lazikani, B. & Pearl, F. M. G. Therapeutic opportunities within the DNA damage response. *Nat. Rev. Cancer* **15**, 166–180 (2015).
75. Álvarez-Quilón, A. et al. Endogenous DNA 3′ blocks are vulnerabilities for BRCA1 and BRCA2 deficiency and are reversed by the APE2 nuclease. *Mol. Cell* **78**, 1152–1165.e8 (2020).
76. Vilhjálmsson, B. J. et al. Modeling linkage disequilibrium increases accuracy of polygenic risk scores. *Am. J. Hum. Genet*. **97**, 576–592 (2015).
77. Purcell, S. et al. PLINK: a tool set for whole-genome association and population-based linkage analyses. *Am. J. Hum. Genet*. **81**, 559–575 (2007).
78. Burgess, S., Butterworth, A. & Thompson, S. G. Mendelian randomization analysis with multiple genetic variants using summarized data. *Genet. Epidemiol*. **37**, 658–665 (2013).
79. Burgess, S. & Thompson, S. G. Interpreting findings from Mendelian randomization using the MR-Egger method. *Eur. J. Epidemiol*. **32**, 377–389 (2017).
80. Bowden, J., Davey Smith, G., Haycock, P. C. & Burgess, S. Consistent estimation in Mendelian randomization with some invalid instruments using a weighted median estimator. *Genet. Epidemiol*. **40**, 304–314 (2016).
81. Bowden, J. et al. Improving the visualization, interpretation and analysis of two-sample summary data Mendelian randomization via the radial plot and radial regression. *Int. J. Epidemiol*. **47**, 2100 (2018).
82. Samuelsson, A.-M. et al. Diet-induced obesity in female mice leads to offspring hyperphagia, adiposity, hypertension, and insulin resistance: a novel murine model of developmental programming. *Hypertension* **51**, 383–392 (2008).
83. Sankar, A. et al. KDM4A regulates the maternal-to-zygotic transition by protecting broad H3K4me3 domains from H3K9me3 invasion in oocytes. *Nat. Cell Biol*. **22**, 380–388 (2020).
84. Li, L. et al. Single-cell RNA-seq analysis maps development of human germline cells and gonadal niche interactions. *Cell Stem Cell* **20**, 858–873.e4 (2017).
85. Zhang, Y. et al. Transcriptome landscape of human folliculogenesis reveals oocyte and granulosa cell interactions. *Mol. Cell* **72**, 1021–1034.e4 (2018).
86. Bolger, A. M., Lohse, M. & Usadel, B. Trimmomatic: a flexible trimmer for Illumina sequence data. *Bioinformatics* **30**, 2114–2120 (2014).
87. Chen, S. et al. AfterQC: automatic filtering, trimming, error removing and quality control for fastq data. *BMC Bioinformatics* **18**, 80 (2017).
88. Pertea, M., Kim, D., Pertea, G. M., Leek, J. T. & Salzberg, S. L. Transcript-level expression analysis of RNA-seq experiments with HISAT, StringTie and Ballgown. *Nat. Protocols* **11**, 1650–1667 (2016).
89. Li, H. et al. The Sequence Alignment/Map format and SAMtools. *Bioinformatics* **25**, 2078–2079 (2009).
90. Takai, H. et al. Chk2-deficient mice exhibit radioresistance and defective p53-mediated transcription. *EMBO J*. **21**, 5195–5205 (2002).
91. Lewandoski, M., Wassarman, K. M. & Martin, G. R. Zp3-cre, a transgenic mouse line for the activation or inactivation of loxP-flanked target genes specifically in the female germ line. *Curr. Biol*. **7**, 148–151 (1997).
92. Lam, M. H., Liu, Q., Elledge, S. J. & Rosen, J. M. Chk1 is haploinsufficient for multiple functions critical to tumor suppression. *Cancer Cell* **6**, 45–59 (2004).
93. Takeo, T. & Nakagata, N. Superovulation using the combined administration of inhibin antiserum and equine chorionic gonadotropin increases the number of ovulated oocytes in C57BL/6 female mice. *PLoS ONE* **10**, e0128330 (2015).
94. Schindelin, J. et al. Fiji: an open-source platform for biological-image analysis. *Nat. Methods* **9**, 676–682 (2012).

Acknowledgements This research was conducted using the UK Biobank resource under application numbers 871 (Exeter) and 9797 (Cambridge). Full individual study acknowledgements can be found in the Supplementary Information. The authors wish to dedicate this work to the memory of Professor P. Solc.

Author contributions All authors reviewed the original and revised manuscripts. Leads on manuscript writing: K.S.R., F.R.D., E.R.H., Anna Murray, I. Roig, J.R.B.P. Central statistical genetics analysis team: K.S.R., F.R.D., Anna Murray, J.R.B.P. Animal model working group: J.H., A.M.-M., C.E.A., L.K., H.A., J.L.T., J.M.G., S.T., E.P.T.H., M.F., Y.H., A.S., A. Pujol, A.J.L., J.A.D., S.E.O., S.H.N., P. Solc, E.R.H., I. Roig. Human oocyte expression working group: A. Azad, V.S., R.B., K.W.O., M.K.H., M.L.G., C.Y., E.R.H. Sample collection, genotyping, phenotyping and individual study analysis: K.S.R., F.R.D., D.J.T., P.F., A. Claringbould, O.B.B., P. Sulem, R.G.W., C.T., M.H., K.L., N.O., P.N.T., P.A., S. Stankovic, P.R.H.J.T., T.U.A., B.Z.A., E.N., I.L.A., A.M.A., K.J.A., A. Augustinsson, S. Bandinelli, C.M.B., R.N.B., H.B., M.W.B., S. Benonisdottir, S. Bergmann, M.B., E.B., S.E.B., M.K.B., D.I.B., N.B., J.A.B., L.B., J.E.B., A. Campbell, H.C., J.E.C., E.C., S.J.C., G.C., M.C., T.C., F.J.C., A. Cox, L.C., S.S.C., F.C., K.C., G.D., E.J.C.N.D, R.D., I.D., E.W.D., J.D., A.M.D., M.D., M.E., T.E., P.A.F., J.D.F., L. Ferrucci, N.F., T.M.F., M.G.-D., M. Mezzavilla, M.G.-C., C.G., G.G.G., H.G., D.F.G., V.G., P.G., C.A.H., N.H., P.H., C. Hayward, C. He, W.H., G.H., J.L.H., J.J.H., F.H., D.H., M.A.I., R.D.J., M.D.R.J., E.M.J., P.K.J., D.K., S.L.R.K., C. Kartsonaki, R.K., C.M.K., I.K., C. Kooperberg, P.K., A.W.K., Z.K., M. La Bianca, G.L., C.L., L.J.L., J.S.E.L., D.A.L., L.L.M., J. Li, A.L., S. Lindstrom, T.L., M. Linet, Y.L., S. Liu, J. Luan, R.M., P.K.E.M., M. Mangino, A. Mannermaa, B. Marco, J. Marten, N.G.M., H.M., B.McK., S.E.M., C. Meisinger, T.M., C. Menni, A. Metspalu, L.M., R.L.M., G.W.M., D.O.M., A. Mulas, A.M.M., Alison Murray, M.A.N., A.N., R.N., T.N., D.R.N., A.F.O., H.O., J.N.P., A.V.P., N.L.P., N.P., A. Peters, U.P., P.D.P.P., O.P., E. Porcu, B.M.P., I. Rahman, G.R., H.S.R., P.M.R., S.M.R., A.R., L.M.R., F.R.R., J.R., I. Rudan, R.R., D.R., C.F.S., E.S., D.P.S., S. Sanna, E.J.S., C. Sarnowski, D. Schlessinger, M.K.S., M.J.S., K.E.S., C. Scott, S. Shekari, A.V.S., B.H.S., J.A.S., R.S., M.C.S., T.D.S., J.J.S., M.S., D. Stöckl, J.B.J.v.M., K. Strauch, U.S., A.J.S., T. Tanaka, L.R.T., A.T., U.P., N.J.T., D.T., M.T., M.A.T., T. Truong, J.T., A.G.U., S.U., C.M.V., V.V., U.V., P.V., H.V., Q.W., N.J.W., C.R.W., D.R.W., A.N.W., K.W., G.W., J.F.W., B.H.R.W., A.W., A.R.W., W.Z., M.Z., Z.C., L. Li, L. Franke, S. Burgess, P.D., T.H.P., K. Stefansson, J.C., Y.T.v.d.S., K.L.L., D.I.C., D.F.E., J.A.V., J.M.M., K.K.O., Anna Murray, J.R.B.P.

Competing interests Full individual study and author disclosures can be found in the Supplementary Information.

Additional information

Supplementary information The online version contains supplementary material available at https://doi.org/10.1038/s41586-021-03779-7.

Correspondence and requests for materials should be addressed to E.R.H., A.M., I.R. or J.R.B.P.

Peer review information *Nature* thanks Heng-Yu Fan and the other, anonymous, reviewer(s) for their contribution to the peer review of this work.

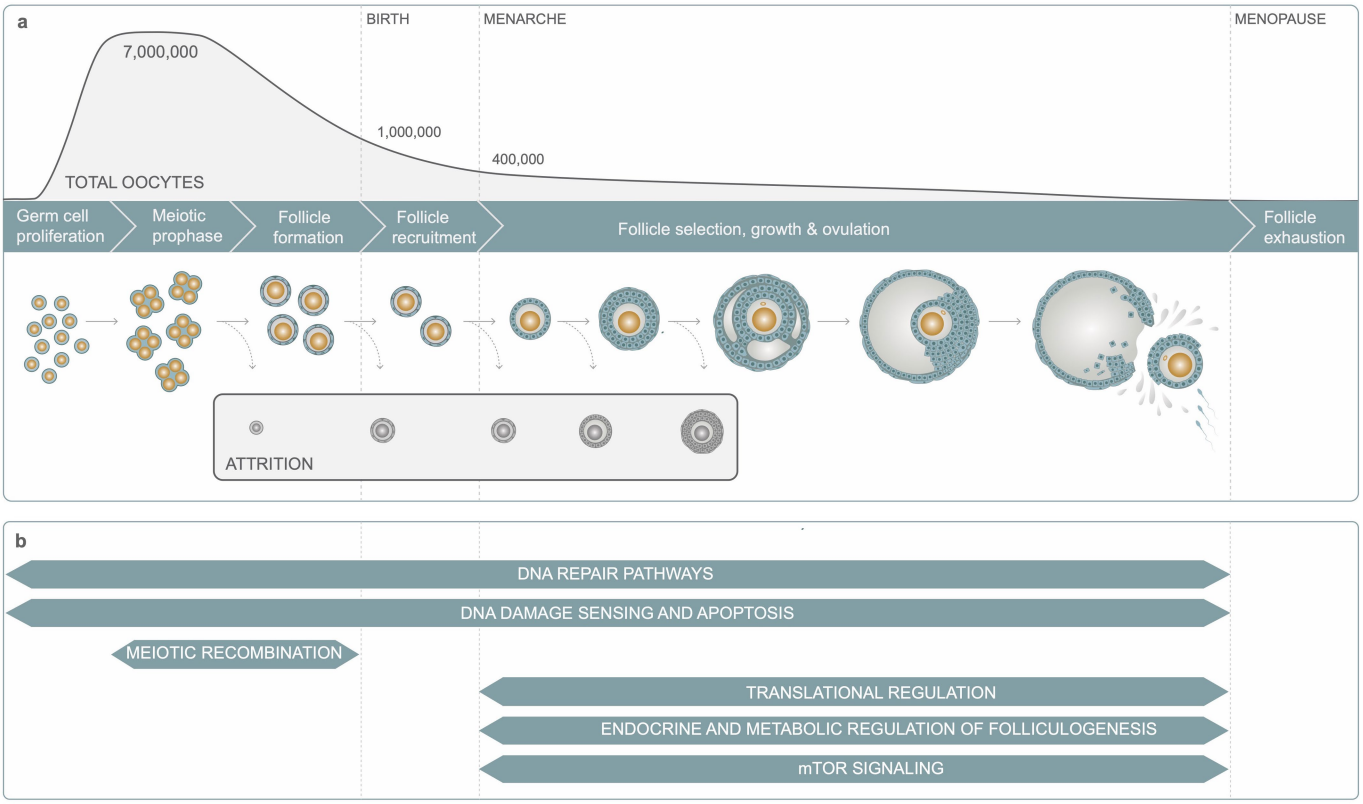

Extended Data Fig. 1 | Overview of ovarian reserve and follicular activity across reproductive life. a, Key processes involved in follicular activity from fetal development to menopause showing the numbers of oocytes at each stage. **b**, Summary of key biological pathways involved in follicular activity and their relationship to stage of reproductive life. Follicles, consisting of oocytes and surrounding granulosa cells, are formed in utero and maintained as resting primordial follicles in the cortex, constituting the ovarian reserve. Follicles are sequentially recruited from the ovarian reserve at a rate of several hundred per month in childhood, peaking at around 900 per month at approximately 15 years of age. Following recruitment, follicles grow by mitotic division of granulosa cells and expansion of oocyte volume for almost six months until meiosis is reinitiated at ovulation and the mature oocyte is released into the oviduct. Waves of atresia (follicle death) accompany developmental transitions and growing follicles are continuously induced to undergo cell death such that, typically, only a single follicle matures to ovulate each month. As ovarian reserve declines, the rate of follicle recruitment decreases, but the preovulatory follicles continue to produce substantial amounts of oestrogen, while other important hormones such as anti-Müllerian hormone and inhibin-B decline, leading to upregulation of the hypothalamus–pituitary gonadal axis.

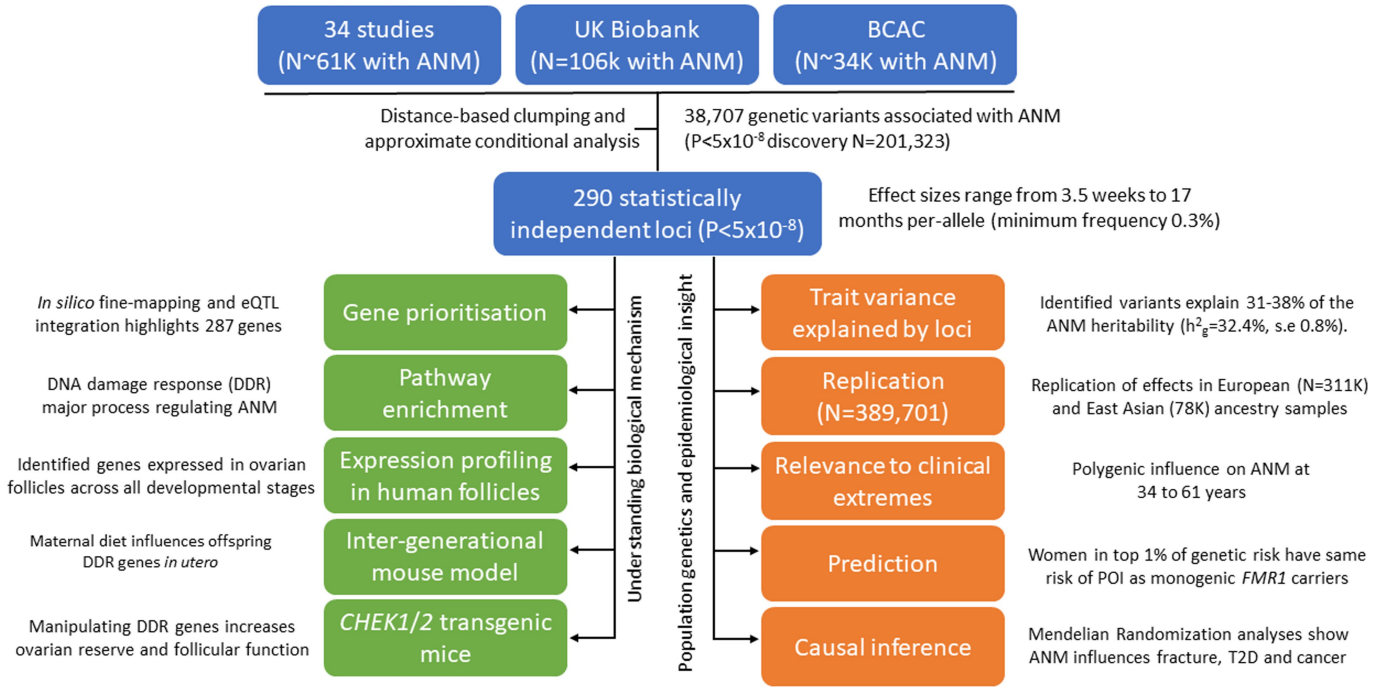

Extended Data Fig. 2 | Overview of performed analyses. Analyses are separated into those intended to lead to understanding of biological mechanisms, and those that lead to insights into population genetics or epidemiology.

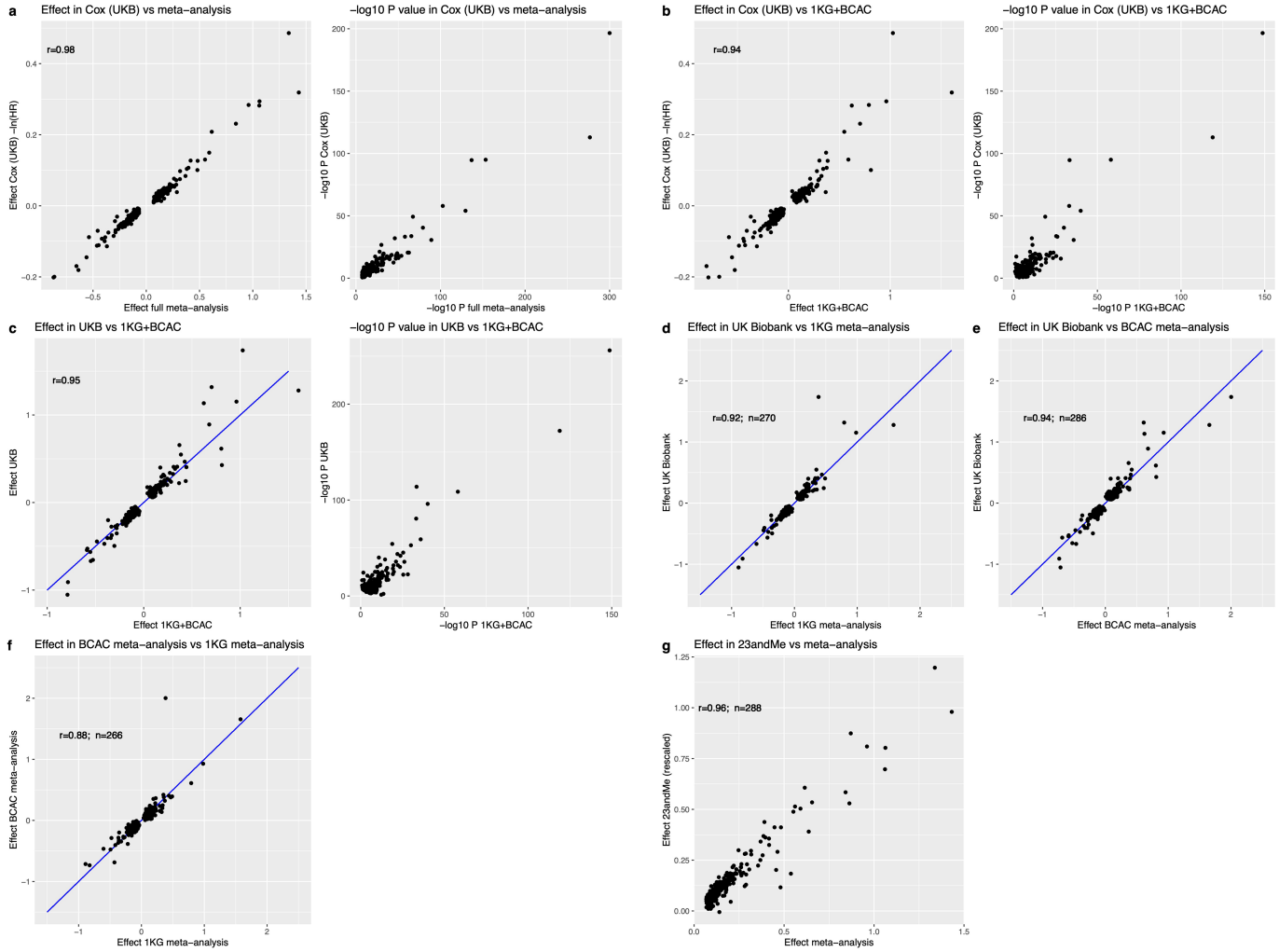

Extended Data Fig. 3 | Consistency of effect estimates across analysis methods and strata. a–**c**, Comparison of effect estimates from: **a**, Cox proportional hazards regression in UK Biobank with linear regression effect estimates from the overall meta-analysis ('Effect full meta-analysis'); **b**, Cox proportional hazards regression in UK Biobank with linear regression effect estimates from the meta-analysis excluding UK Biobank ('Effect 1KG+BCAC'); **c**, linear regression in UK Biobank with linear regression effect estimates from the meta-analysis excluding UK Biobank ('Effect 1KG+BCAC'). **d**–**g**, Comparison of linear regression effect estimates from: **d**, UK Biobank GWAS versus the meta-analysis of 1000 Genomes imputed studies; **e**, UK Biobank GWAS versus meta-analysis of samples from the Breast Cancer Association Consortium (BCAC); **f**, meta-analysis of BCAC samples versus the meta-analysis of 1000 Genomes imputed studies; **g**, 23andMe replication analysis (rescaled) versus overall meta-analysis. HR, hazard ratio from Cox proportional hazards model; *r*, Pearson correlation coefficient; blue line is $y = x$ for reference. Note: *P* values $<1\times10^{-300}$ are shown as 1×10^{-300}.

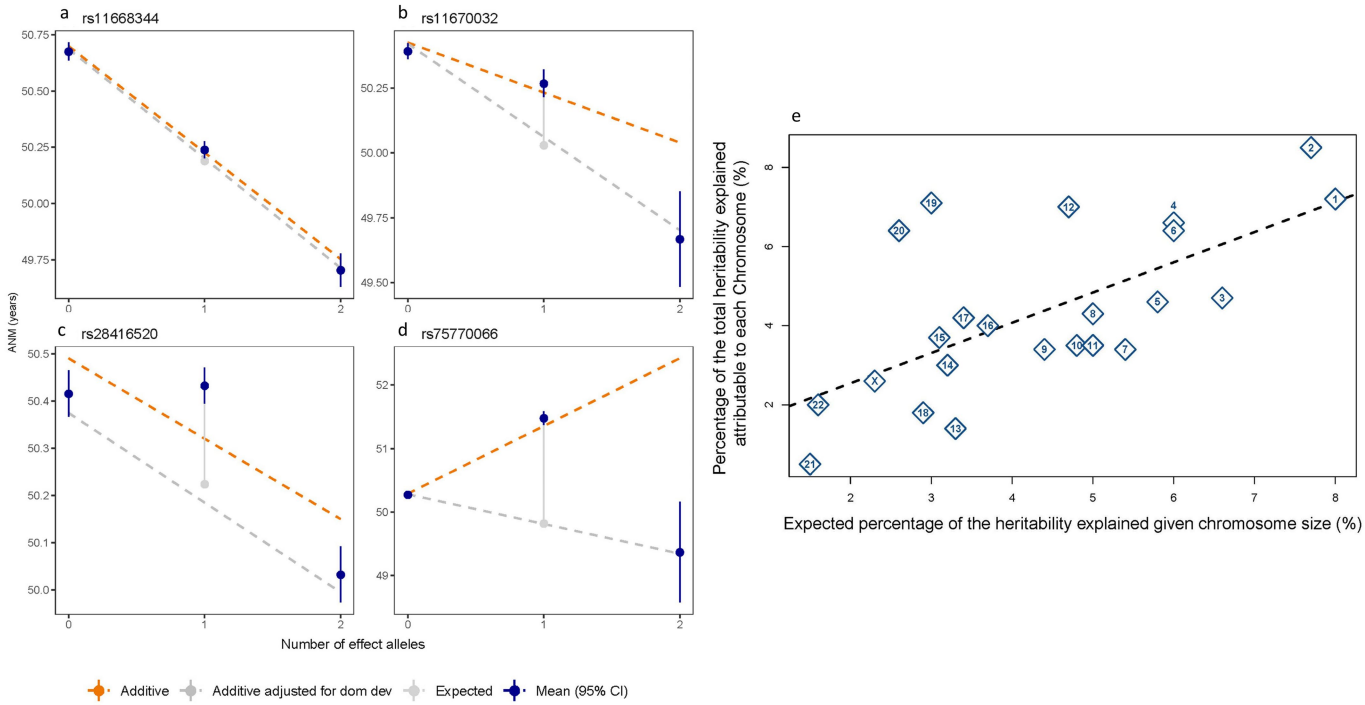

Extended Data Fig. 4 | Deviation from additive effects and distribution of estimated heritability across chromosomes. a–**d**, Genome-wide significant signals showing departure from an additive model. We tested the identified signals for departure from an additive allelic model. **a**, rs11668344 shows no deviation from an additive allelic model, **b**, **c**, rs11670032 (**b**) and rs28416520 (**c**) show deviation from the additive allelic model and a recessive effect. **d**, rs75770066 shows a heterozygote effect. The mean and 95% confidence interval around the mean estimate are shown for each genotype. The expected mean ANM for the heterozygotes is the average of the mean ANM in the homozygote groups. The dashed orange line shows the effect estimate by genotype from linear regression based on an additive allelic model. Estimated ANM for each genotype was calculated as constant from regression model + number alleles × effect estimate from regression model. The dashed grey line indicates the additive effect estimate by genotype from a model adjusting for the dominance deviation effect of the heterozygote group (solid grey line). All regression models were adjusted for centre, genotyping chip and genetic principal components. dom dev, dominance deviation. **e**, The percentage of the total heritability explained that was attributable to each chromosome (observed heritability) is compared with the expected proportion calculated on the basis of chromosome size. The heritability of ANM was not uniformly distributed across chromosomes in proportion to their size. The X chromosome did not explain more heritability than expected given its size, but chromosome 19 explained 2.36% (1.98–2.75) of the trait variance—greater than the individual contributions of nearly all larger chromosomes (weighted average for chromosomes 1–18: 1.7%, s.e 0.2%) and about 2.5 times more than expected given its size. This was partially attributable to a single locus at 19q13 which explained about 0.75% of trait variance and where we mapped six independent signals (Supplementary Table 2). The dashed line shows the mean ratio of expected to observed heritability across all chromosomes. Chromosome size was estimated based on the number of genetic variants.

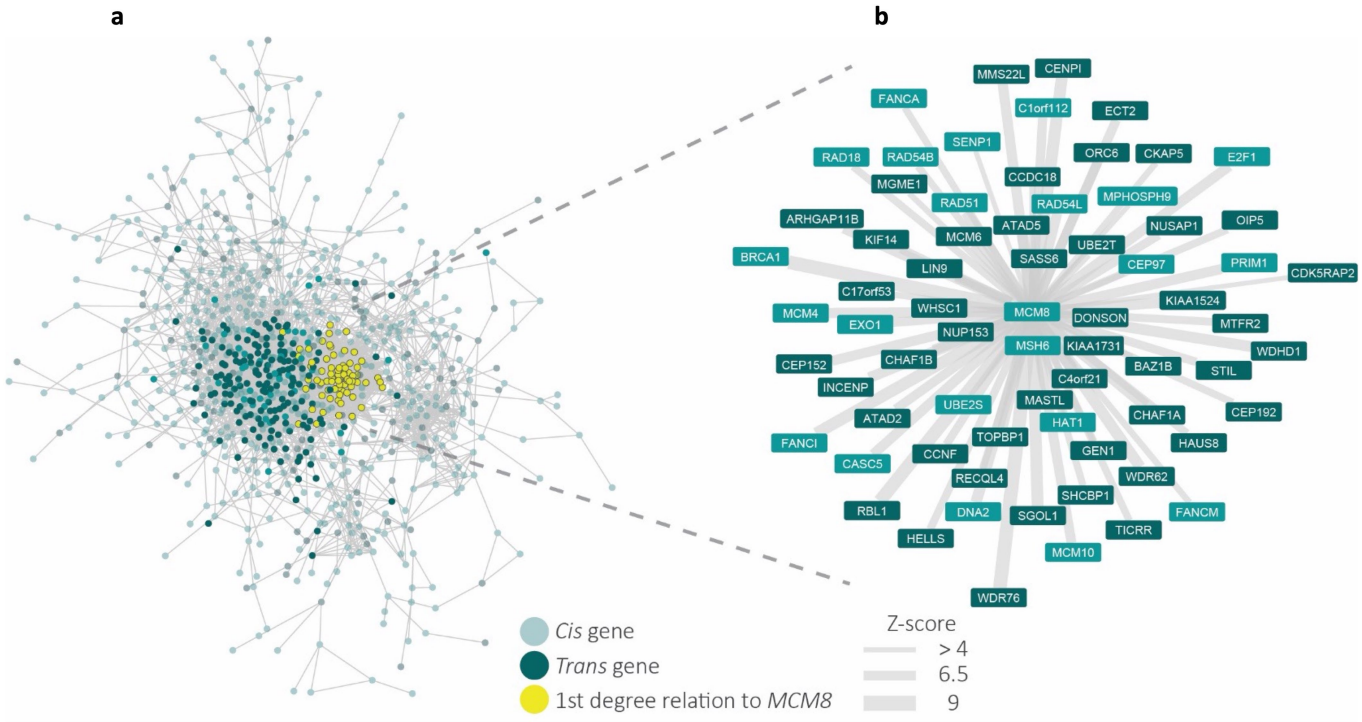

Extended Data Fig. 5 | Gene co-regulation networks for age at menopause genes with *MCM8* highlighted. a, Gene co-regulation network for genes relating to age at menopause. Nodes indicate genes that are either in a *cis* region from the GWAS or have been prioritized by Downstreamer; edges indicate a co-regulation relationship with a *z*-score > 4. Co-regulation is defined as the Pearson correlation between genes in a scaled eigenvector matrix derived from a multi-tissue gene network[72]. *cis* genes are defined as genes that are within 300 kb of a GWAS top hit for age at menopause. *trans* genes are defined as having been prioritized by Downstreamer's co-regulation analysis and not being within 300 kb of a GWAS top hit. Downstreamer prioritizes genes by associating the gene *P* value profile of the GWAS (calculated using PASCAL[71]) to the co-regulation profile of each protein-coding gene. Only genes for which this association passes Bonferroni significance are shown as *trans* genes. Teal, *cis* genes; dark teal, *trans* genes; yellow, genes with a first-degree relation to *MCM8*. **b**, Gene co-regulation network showing the genes that have a first-degree relationship with *MCM8* with a *z*-score > 4. Edge width indicates the *z*-score of the co-regulation relationship. Colours as in **a**, with the exception of yellow, as all genes have a first-degree relation to *MCM8*.

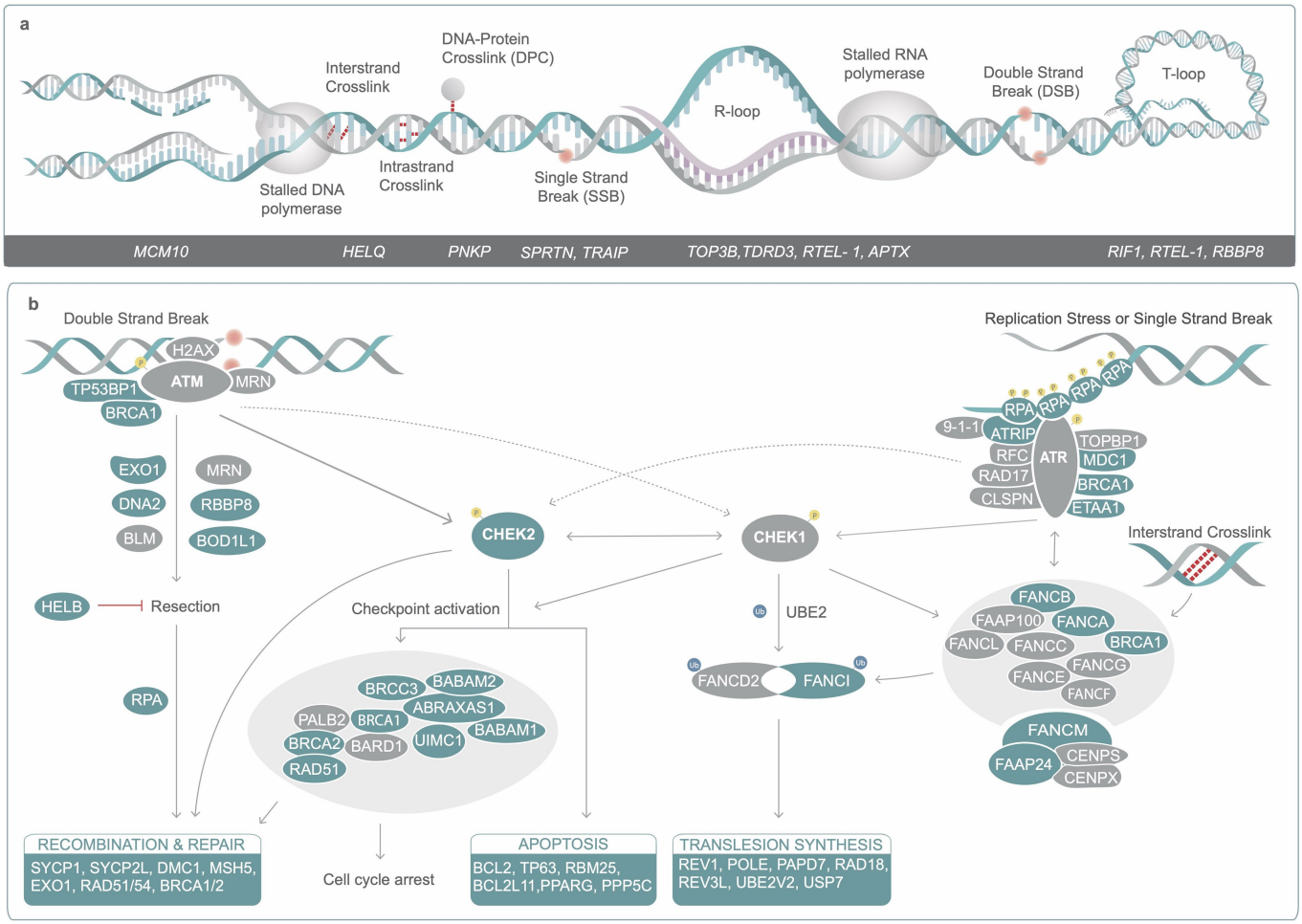

Extended Data Fig. 6 | DNA damage response and repair pathways implicated in reproductive ageing in humans. a, Consequences of replication stress annotated with genes involved that were within 300 kb of the ANM signals. **b**, Genes involved in downstream DNA damage response and repair pathways with those within 300 kb of an ANM signal shown in blue. A full list of genes involved in DNA damage response and apoptosis annotated with genome-wide signals for ANM is provided in Supplementary Table 19. MRN, *MRN–MRE11–RAD50–NBS1* complex; RPA, replication protein A including a subunit encoded by *RPA1*; RFC, replication factor C including a subunit encoded by *RFC1*; 9-1-1, *RAD9–HUS1–RAD1* complex.

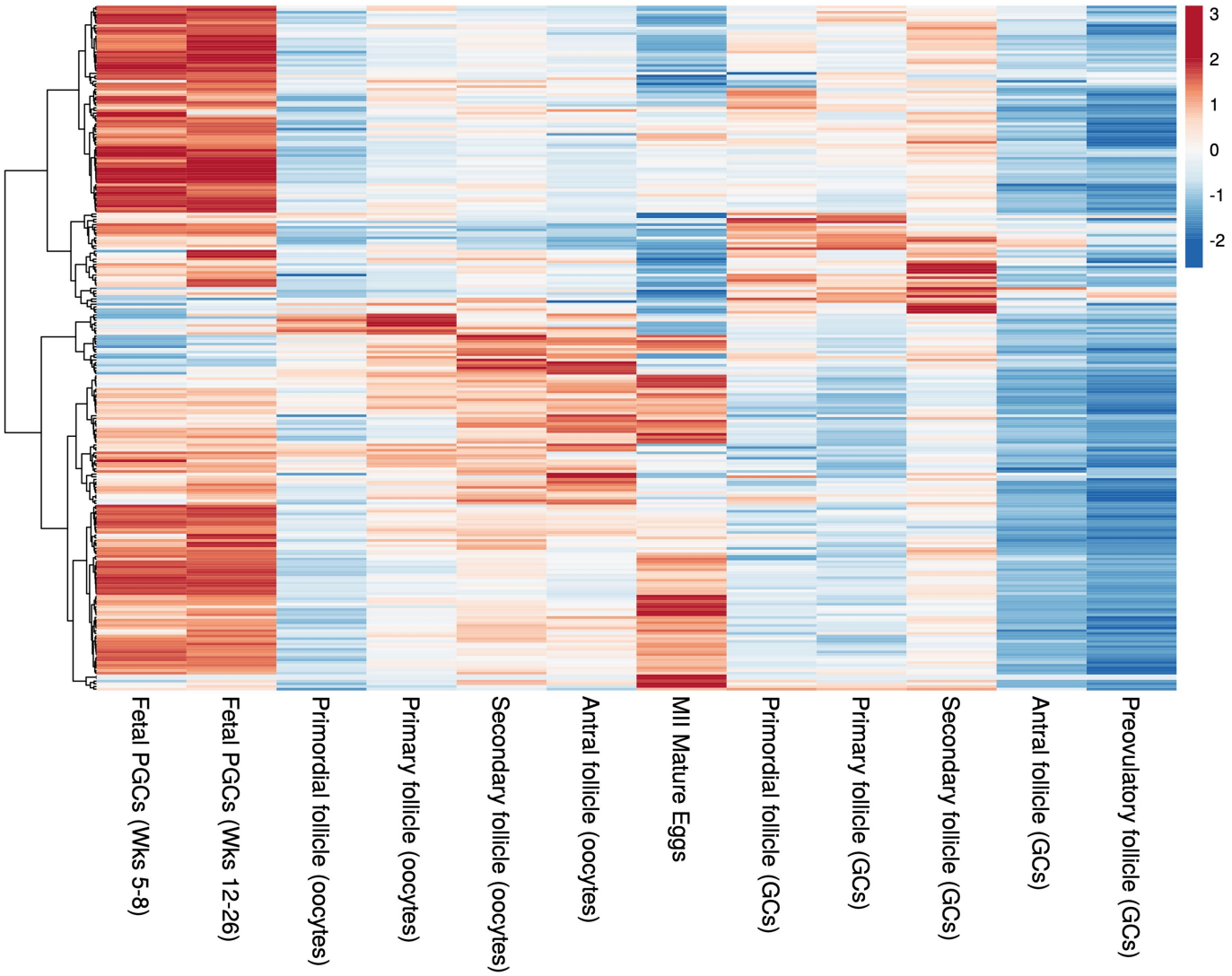

Extended Data Fig. 7 | Cluster plot of expression of consensus genes identified from the genome-wide analyses in germ cells across different developmental stages. Genes were selected from the GWAS signals, based on in silico prioritization (Supplementary Table 5). Of the 283 consensus genes highlighted by the GWAS, 258 passed QC and were available in the expression dataset. Gene expression was measured in human fetal primordial germ cells[84,85] and in oocytes and granulosa cells in adult follicles (dataset generated in this study). Plot shows *z*-scores, calculated by subtracting the mean TPM in all samples for a gene and dividing by the s.d. GC, granulosa cell; MII, meiosis II; PGC, primordial germ cell; Wks, weeks.

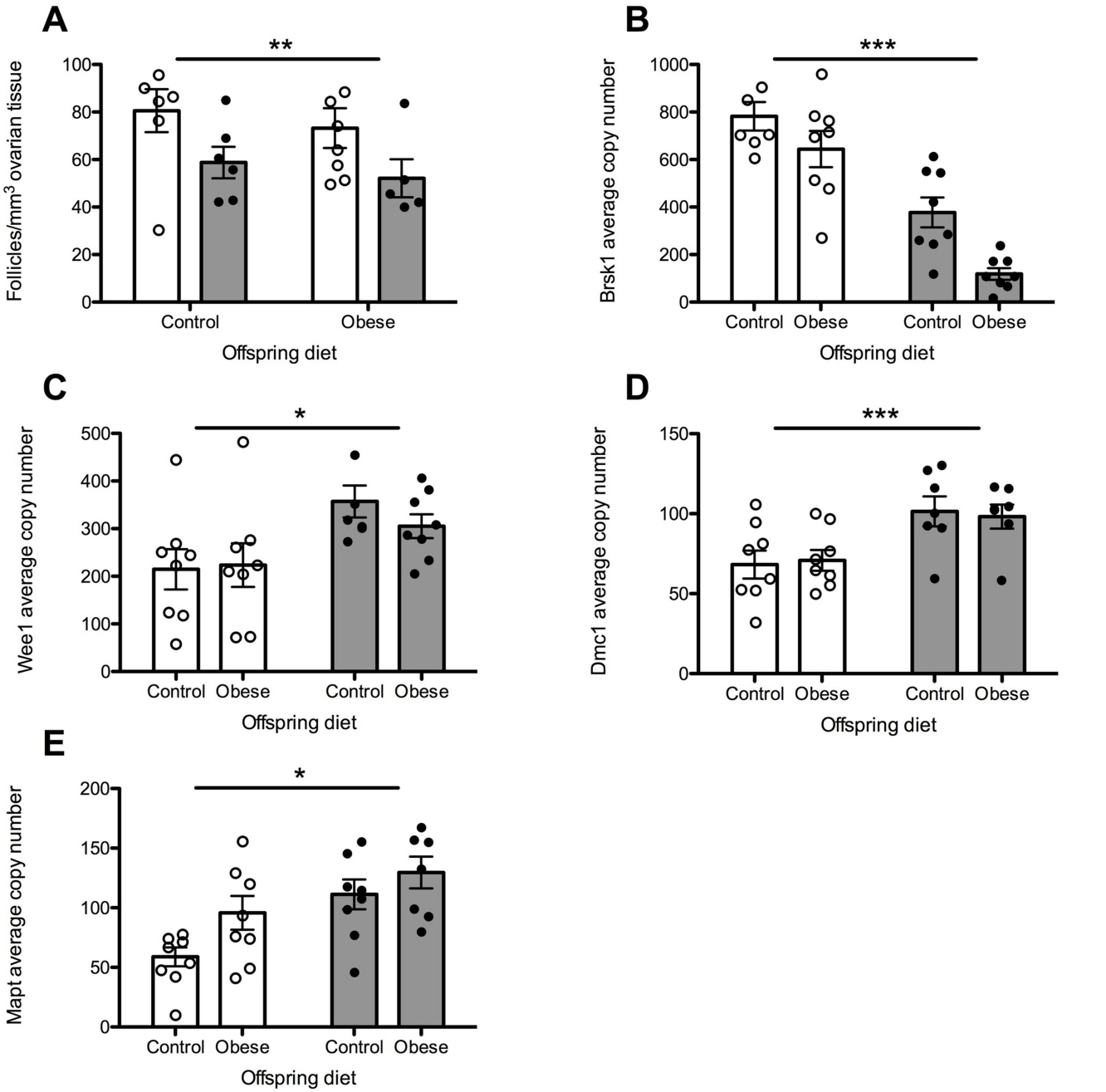

Extended Data Fig. 8 | Relationship between decreased ovarian reserve and gene expression. Open bar/dot groups: control maternal diet, normal ovarian reserve. Grey bar/dot groups: obesogenic maternal diet, reduced ovarian reserve. Dots, individual observations. Bar heights and error bars: mean ± s.e.m. **a**, Ovarian follicular reserve in young adulthood in wild-type mice. Total follicles per mm^3 ovarian tissue at 12 weeks. $n = 8$ biologically independent animals from different litters in each group. $P = 0.0091$. **b**, *Brsk1* expression in the same mice, measured using qRT–PCR and expressed as average copy number. $P = 0.0001$. **c**, *Wee1* expression in the same mice, measured using qRT–PCR and expressed as average copy number. $P = 0.0256$. **d**, *Dmc1* expression in the same mice, measured using qRT–PCR and expressed as average copy number. $P = 0.00001$. **e**, *Mapt* expression in the same mice, measured using qRT-PCR and expressed as average copy number. $P = 0.0378$. All panels, two-way ANOVA after correction for multiple hypothesis testing. $^*P < 0.05$, $^{**}P < 0.01$, $^{***}P < 0.001$.

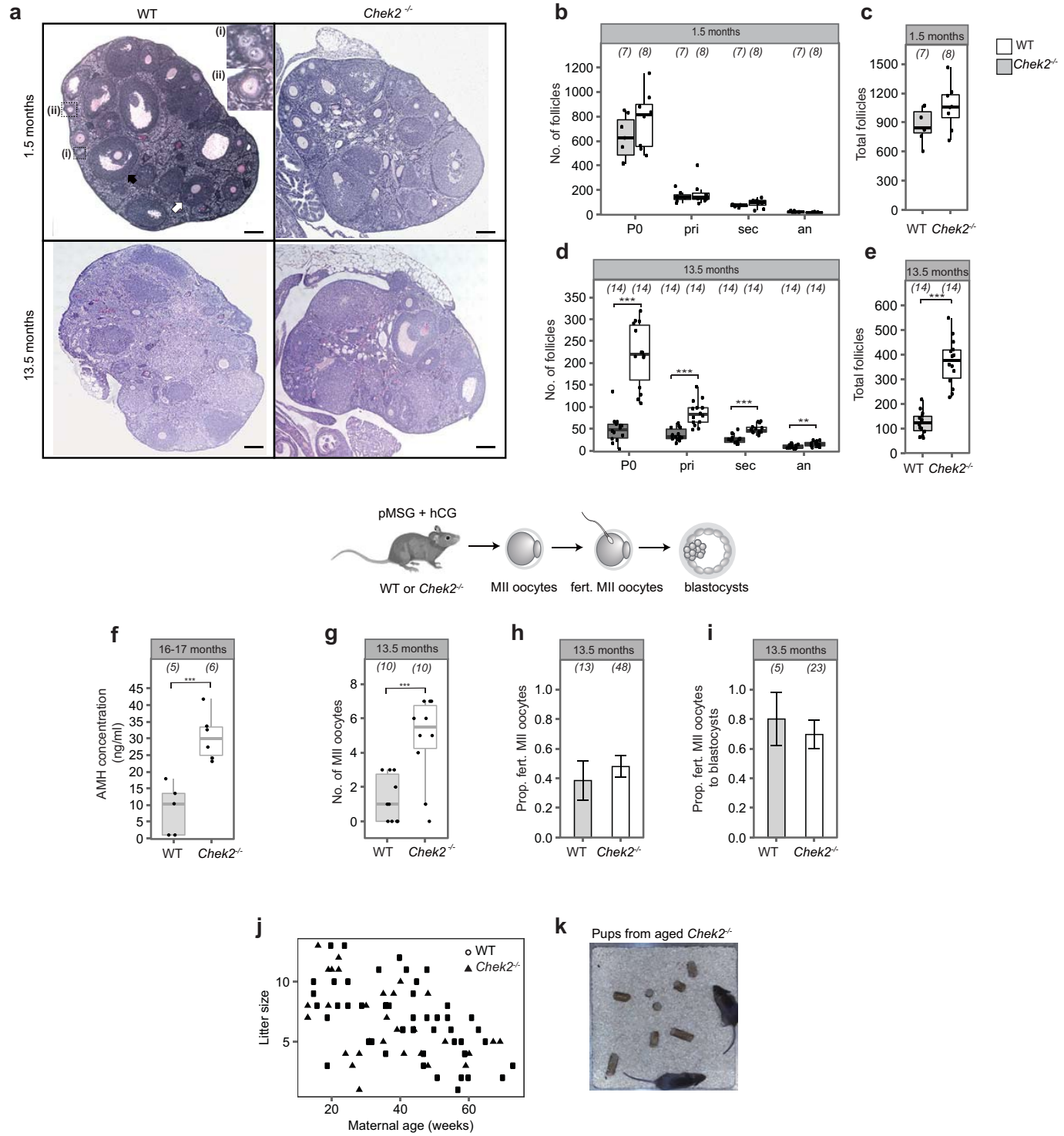

Extended Data Fig. 9 | *Chek2* deletion increases reproductive lifespan in mouse. a, Representative images of ovarian sections of 1.5- and 13.5-month-old wild-type (WT) and *Chek2*$^{-/-}$ mice stained with PAS-haematoxylin. Primordial follicles (inset (i)), primary follicles (inset (ii)), secondary follicle (white arrow) and antral follicle (black arrow) are shown. Scale bars, 200 µm. **b**–**e**, Number of follicles (by class and total) present in WT and *Chek2*$^{-/-}$ mouse ovaries. **b**, **c**, 1.5 months old; **d**, **e**, 13.5 months old. Numbers in parentheses show the total number of ovaries analysed. **f**, Serum AMH (ng ml^{-1}) in 16–17-month-old *Chek2*$^{-/-}$ mice. Numbers in parentheses show the number of mice assessed. **g**–**i**, Gonadotrophin stimulation of 13.5-month-old females. Numbers in parentheses show: **g**, the number of MII oocytes retrieved per female; **h**, the number of MII oocytes fertilized; and **i**, the number of fertilized oocytes assessed for blastocyst formation. **j**, Litter size of WT and *Chek2*$^{-/-}$ females throughout the reproductive lifespan. Litter sizes from nine WT and five *Chek2*$^{-/-}$ females are shown. Breeding cages contained one male and one female. Generalized linear model analysis showed maternal age effect, but no effect of genotype on litter sizes. **k**, Image of healthy pups born to 13 month-old *Chek2*$^{-/-}$ females. **b**–**i**, Two-sample *t*-test and Fisher's exact test were used to compare WT and *Chek2*$^{-/-}$ for statistical significance: $^{*}P < 0.05$, $^{**}P < 0.025$, $^{***}P < 0.001$. All *P* values are two-sided. Error bars indicate s.e.m. For box plots: centre line, median; box limits, IQR; whiskers, 1.5 × IQR (**b**–**g**). an, antral follicle; pri, primary follicle; P0, primordial follicle; sec, secondary follicle. Mouse strain: maintained on a mixed background, C57BL/6 129Sv, accession number BRC03481 at the RIKEN Bioresource Centre.

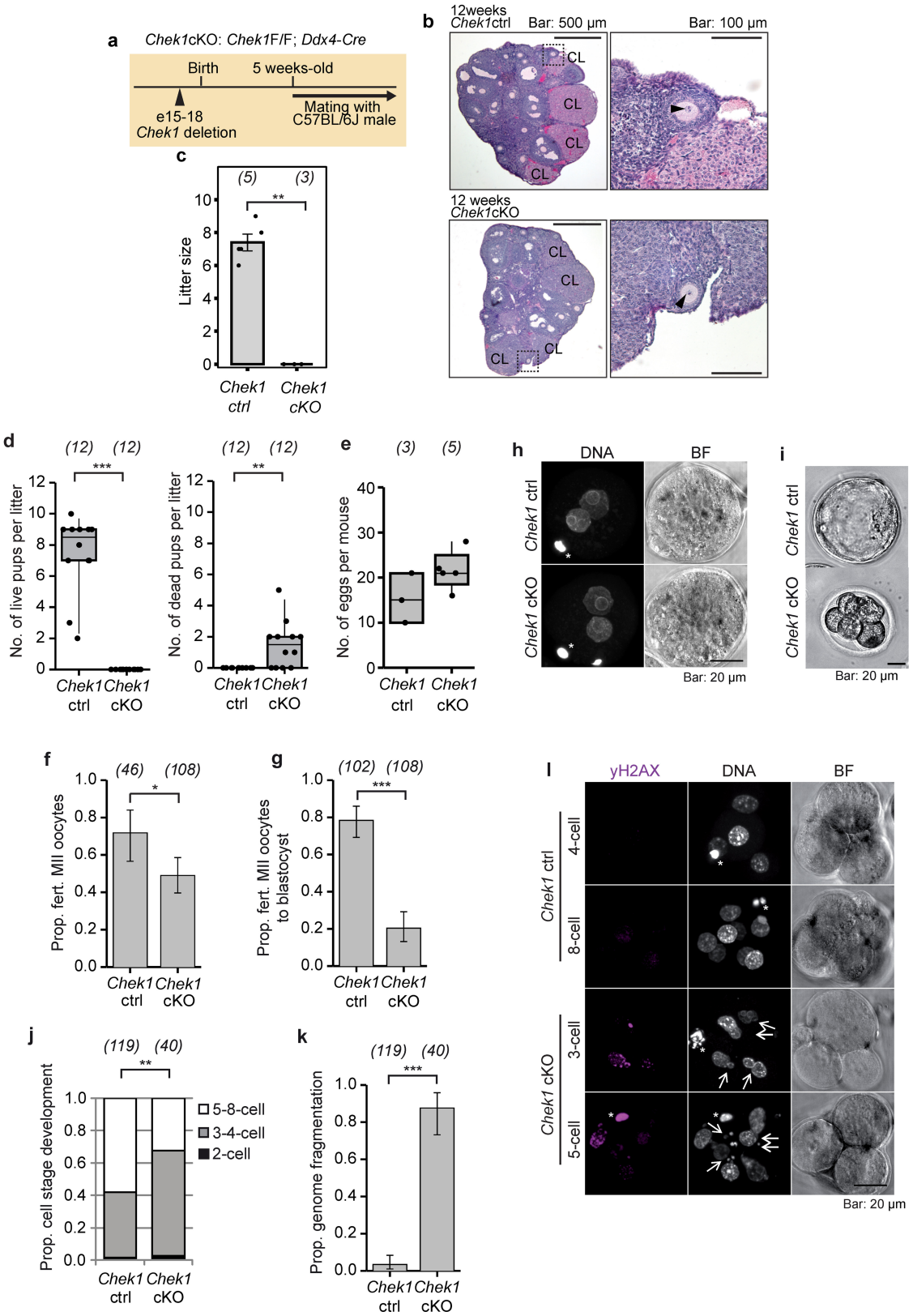

Extended Data Fig. 10 | See next page for caption.

Extended Data Fig. 10 | Conditional knockout *Chek1* females are infertile due to requirement for *Chek1* during preimplantation embryo development. a, Schematic of generation of conditional knockout mouse model of *Chek1* (*Chek1* cKO) in the female germline using *Ddx4-Cre*. A similar approach was used for *Zp3-Cre*. **b**, In ovarian sections stained with H&E, we found follicles, corpora lutea (CL) and oocytes which contain nuclear structures (arrowheads, magnified right panels). These findings suggest that oestrus cycles and ovulation followed by corpus luteum formation are independent of *Chek1* disruption in oocytes in vivo. **c**, Litter size of *Chek1* cKO females. Three females older than 5 weeks of age were mated with C57BL/6J males. Five independent littermate females (F/+, Tg−/Tg−; F/F, Tg−/Tg−; or F/+, Tg+/Tg−) were used as *Chek1* controls (ctrl). While *Chek1* control females delivered normally, *Chek1* cKO females delivered no litters (Mann–Whitney test, $^{**}P = 0.0179$). Thus, these results indicate that *CHEK1* is essential in the female germline. **d**, Litter size of *Chek1*-cKO and control females using the *Zp3-Cre* during follicular growth. Three-month-old control (*Chek1* F/F; *Chek1* ctrl, $n = 4$) and conditional knockout (*Chek1* F/F; *Chek1* cKO with *Zp3-Cre*, $n = 4$) were consecutively mated three times with wild-type ($Chek1^{+/+}$) males, and the number of live (left) and dead (right) pups was monitored. While C*hek1* ctrl females delivered a normal number of live pups, *Chek1* cKO females had only a reduced number of perinatally dead pups (Mann–Whitney *U*-test: $^{***}P < 0.001$, $^{**}P < 0.01$). Numbers in parentheses show the number of litters. **e**, The mean number of all ovulated eggs (sum of MII oocytes and fertilized MII oocytes) per mouse with s.e.m. (Mann–Whitney *U*-test, $P = 0.126$). Each data point represents the number of eggs per mouse. Three- to five-month-old C*hek1* ctrl ($n = 3$) and *Chek1* cKO ($n = 5$) females were mated with wild-type ($Chek1^{+/+}$) males after pMSG + hCG stimulation. The number of ovulated eggs isolated 18 h after hCG stimulation and additional 10 h cultured in vitro was scored. The number of mice is shown in parentheses. **f**, The proportion of fertilized MII oocytes to all ovulated eggs with a binomial confidence interval (Fisher's exact test, $^{*}P = 0.012$; 95% CI 1.9–6.0; OR, 2.62). Numbers in parentheses show the total number of analysed eggs. **g**, The proportion of embryos that developed to blastocysts with binomial confidence interval (Fisher's exact test, $^{***}P < 0.0001$). Fertilized MII oocytes (zygotes) were isolated from females stimulated with pMSG + hCG 18 h after hCG administration and cultured in vitro for 96 h (approximately embryonic day (E)3.5) when development to blastocyst was scored. Data are pooled from four independent experiments. The number of embryos is shown in parentheses. **h**, Fertilized eggs from C*hek1* ctrl ($n = 18$) and *Chek1* cKO ($n = 13$) females were fixed and stained for DNA (DAPI). All fertilized eggs from both genotypes showed normal pronucleus formation. The data were pooled from two independent experiments. Asterisks, polar bodies. **i**, The majority of C*hek1* ctrl embryos formed blastocysts (**g**), but *Chek1* cKO embryos were arrested mainly at the 3–8-cell stages. Representative bright-field images are shown. **j**, Proportion of developmental stages 2 cell, 3–4 cell and 5–8 cell (Cochran–Armitage trend test, $^{**}P = 0.0073$). *Chek1* ctrl and *Chek1* cKO zygotes were isolated from 13 C*hek1* ctrl and 6 *Chek1* cKO females stimulated with pMSG + hCG 18 h after hCG administration and cultured in vitro for 49 h. Embryos were fixed and stained for γH2AX by immunofluorescence. DNA was visualized by DAPI (**l**). **k**, Proportion of embryos with genome fragmentation with binomial confidence interval (Fisher's exact test, $^{***}P < 0.0001$). Data are pooled from two independent experiments. The number of embryos is shown in parentheses. **l**, *Chek1* ctrl and *Chek1* cKO zygotes (**j**, **k**) were fixed and stained for γH2AX (magenta) by immunofluorescence. DNA (grey) was visualized by DAPI. Arrows, genome fragments; asterisks, polar bodies. These findings suggest that maternally expressed *Chek1* is critical for genome integrity protection during first divisions of preimplantation embryos in mice. All *P* values are two sided. For box plots: centre line, median; box limits, IQR; whiskers, 1.5 × IQR. Strains: C57BL/6-FVB mixed background for **a**–**c** (*Chek1* cKO, *Ddx4-Cre*); C57BL6-CD1 mixed background (*Chek1* cKO, *Zp3-Cre*) for **d**–**l**.

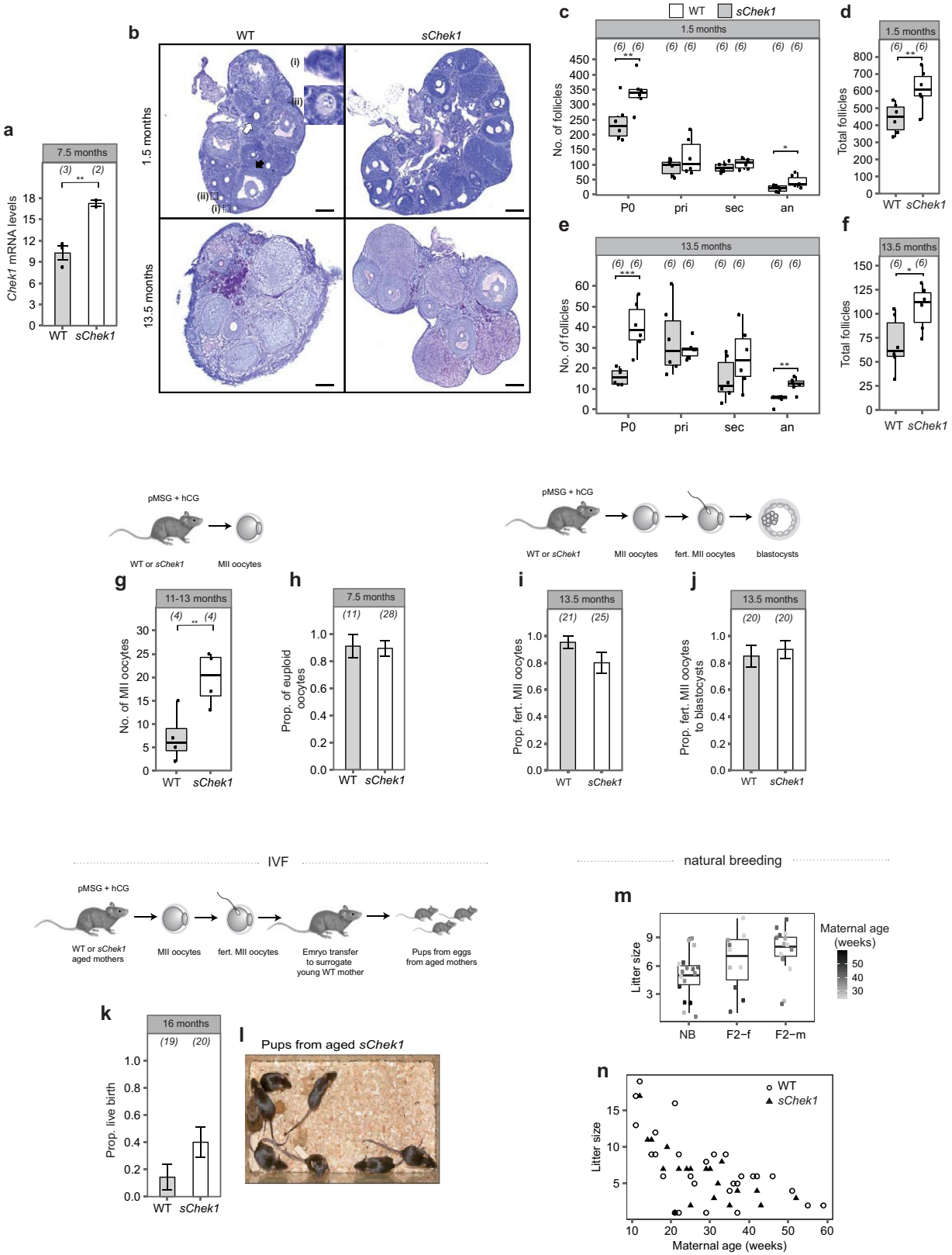

Extended Data Fig. 11 | See next page for caption.

Extended Data Fig. 11 | Extended reproductive lifespan in females carrying an extra copy of *Chek1* (*sChek1*). **a**, mRNA expression levels of *Chek1* in oocytes; numbers in parentheses show the number of mice stimulated for retrieval of oocytes. **b**, Representative images of ovarian sections from 1.5- and 13.5-month-old wild-type (WT) and *sChek1* mice stained with PAS-haematoxylin. Primordial follicles (inset (i)), primary follicles (inset (ii)), secondary follicle (white arrow) and antral follicle (black arrow) are shown. Scale bars, 200 µm. **c**–**f**, Numbers of follicles (by class and total) in WT and *sChek1* littermates: **c**, **d**, 1.5 months old; **e**, **f**, 13.5 months old. Numbers in parentheses show the total number of ovaries analysed. **g**–**j**, MII oocytes retrieved in response to pMSG and hCG (**g**), proportion of euploid oocytes (**h**), proportion fertilized (**i**) and proportion developed to blastocysts (**j**) at different ages of WT and *sChek1* mice. Numbers in parentheses show: **g**, the number of female mice stimulated for retrieval of oocytes; **h**, the number of oocytes assessed for aneuploidy; **i**, the number of MII oocytes fertilized; and **j**, the number of fertilized oocytes assessed for blastocyst development. **k**, Proportion of live births relative to transferred embryos from in vitro fertilized oocytes from aged mice (16 months); numbers in parentheses show the number of embryos transferred. **l**, Healthy pups born to 16-month-old *sChek1* females after IVF. **m**, Litter sizes from F2 females or males from aged *sChek1* females after IVF treatment in **k**, compared to females of equivalent ages that were naturally breeding. Note that for natural breeding there were two females and one male per breeding cage, whereas F2 cages contained a single male and one female. Therefore, litter sizes are an underestimate for the IVF-conceived pups. **n**, Litter sizes of WT and *sChek1* females throughout their reproductive lifespan. Data are from six breeding cages, three for each genotype. Each breeding cage contained one WT male and two females that were either WT or *sChek1*. Generalized linear model analysis showed maternal age effect, but no effect of genotype on litter sizes. **a**–**k**, Two-sample *t*-test and Fisher's exact test were used to compare WT and s*Chek1* for statistical significance: $^{*}P < 0.05$, $^{**}P < 0.025$, $^{***}P < 0.001$. All *P*-values are two sided. Error bars indicate s.e.m. For box plots: centre line, median; box limits, IQR; whiskers, 1.5 × IQR (**c**–**g**, **m**). NB, natural breeding; F2-f, F2 female; F2-m, F2 male. Mouse strain: inbred from mixed background C57BL/6 129Sv.

nature research

Corresponding author(s): Eva R Hoffmann, Anna Murray, Ignasi Roig, John R B Perry

Last updated by author(s): May 28, 2021

Reporting Summary

Nature Research wishes to improve the reproducibility of the work that we publish. This form provides structure for consistency and transparency in reporting. For further information on Nature Research policies, see our Editorial Policies and the Editorial Policy Checklist.

Statistics

For all statistical analyses, confirm that the following items are present in the figure legend, table legend, main text, or Methods section.

n/a	Confirmed	
☐	☒	The exact sample size (*n*) for each experimental group/condition, given as a discrete number and unit of measurement
☐	☒	A statement on whether measurements were taken from distinct samples or whether the same sample was measured repeatedly
☐	☒	The statistical test(s) used AND whether they are one- or two-sided *Only common tests should be described solely by name; describe more complex techniques in the Methods section.*
☐	☒	A description of all covariates tested
☐	☒	A description of any assumptions or corrections, such as tests of normality and adjustment for multiple comparisons
☐	☒	A full description of the statistical parameters including central tendency (e.g. means) or other basic estimates (e.g. regression coefficient) AND variation (e.g. standard deviation) or associated estimates of uncertainty (e.g. confidence intervals)
☐	☒	For null hypothesis testing, the test statistic (e.g. *F*, *t*, *r*) with confidence intervals, effect sizes, degrees of freedom and *P* value noted *Give P values as exact values whenever suitable.*
☒	☐	For Bayesian analysis, information on the choice of priors and Markov chain Monte Carlo settings
☒	☐	For hierarchical and complex designs, identification of the appropriate level for tests and full reporting of outcomes
☐	☒	Estimates of effect sizes (e.g. Cohen's *d*, Pearson's *r*), indicating how they were calculated

Our web collection on statistics for biologists contains articles on many of the points above.

Software and code

Policy information about availability of computer code

Data collection	Details of software used by each study included in genome-wide meta-analyses (as listed in Supplementary Table 1 and main text): BOLT-LMM (v2.3.2, v2.3.4), EPACTS, GEMMA v0.94.1, GenABEL, ProbABEL (v0.4.5), IMPUTE, MACH2QTL, matlab, MiniMac, Plinkv1.07, PLINKv1.9, QUICKTEST 0.95, R, RareMetalWorker, SNPTest (v2, v2.5), SHAPEIT3, IMPUTE2, IMPUTE4. Some studies used in-house genome-wide analysis code which was study specific and so is not available. References are provided in the Methods for where software/code can be accessed. Specific versions of software (e.g. R) are listed where information was supplied by studies. RNA Seq data was processed using bcl2fastq2 Conversion Software v2.19, trimmomatic v0.36, hisat2, samtools, picard metrics, picard tools, Stringtie.
Data analysis	METAL; GCTA; Stata v14, v16; BOLT-LMM; LOFTEE; IGV; Variant Effect Predictor b38; PLINK v1.9, v1.90b4.4; SMR; DEPICT; LDSC-SEG; MAGENTA; Excel; SAIGE-GENE; LOFTEE; UCSC Liftover; Downstreamer; MAGMAv1.08; LDPRED; Radial-MR; R (v2.14.1). References are provided in the Methods for where software/code can be accessed.

For manuscripts utilizing custom algorithms or software that are central to the research but not yet described in published literature, software must be made available to editors and reviewers. We strongly encourage code deposition in a community repository (e.g. GitHub). See the Nature Research guidelines for submitting code & software for further information.

Data

Policy information about availability of data

All manuscripts must include a data availability statement. This statement should provide the following information, where applicable:

- Accession codes, unique identifiers, or web links for publicly available datasets
- A list of figures that have associated raw data
- A description of any restrictions on data availability

Data availability statement:
Full genome-wide association summary statistics for the discovery meta-analysis are available from the ReproGen website (www.reprogen.org).
MII Oocyte dataset EGAS00001004947
SMR https://cnsgenomics.com/software/smr/#eQTLsummarydata
Tabula Muris https://tabula-muris.ds.czbiohub.org/
LDSC-SEG https://github.com/bulik/ldsc/wiki/Cell-type-specific-analyses
RNA-seq samples https://www.ebi.ac.uk/ena
Human oocyte expression analyses: GSE107746, GSE107746

Source data for Fig. 1 are available from the ReproGen website.
Source data for Fig. 2-3; Extended Data Fig. 4, 8-10 are available.

Field-specific reporting

Please select the one below that is the best fit for your research. If you are not sure, read the appropriate sections before making your selection.

☒ Life sciences ☐ Behavioural & social sciences ☐ Ecological, evolutionary & environmental sciences

For a reference copy of the document with all sections, see nature.com/documents/nr-reporting-summary-flat.pdf

Life sciences study design

All studies must disclose on these points even when the disclosure is negative.

Sample size	Genome-wide meta-analyses were performed using all available study cohorts who agreed to participate. This was an increase in the sample size compared with previous published analyses that identified 56 genetic signals (n=70,000 vs n=200,000, Day, F.R. et al. Nat. Genet. 10, 1–19 (2017)). Similarly, the Mendelian Randomization (MR) analyses used the largest available GWAS summary statistics. We have previously demonstrated the ability to detect causal relationships based on summary statistics from smaller GWAS sample sizes. For the mouse model of environmentally-induced low ovarian reserve, power was determined based on effect sizes for gene expression differences observed in Aiken et al FASEB J. 30, 1548–56 (2016).
Data exclusions	For genome-wide meta-analyses, standard quality control criteria were applied by two analysts independently and only studies passing these checks were included in the meta-analyses. Within each individual study contributing genetic data, standard genotype qc protocols were followed.
Replication	A sample of 294,828 women from 23andMe, Inc was used as a replication cohort. We observed high concordance in effect estimates for the 290 signals identified in our main results with the replication analyses with nearly all variants at least nominally associated. We also evaluated the 290 signals identified by our main analyses in 78,317 women of East Asian ancestry, finding broad replication, consistent with previous observations (PMID: 29773799). Pathway and enrichment analyses were carried out using multiple software packages to explore consistency of results. Gene expression analyses in human oocytes were based on z-scores to enable comparison between data sources. The MII Oocytes single-cell RNA-seq dataset generated in this study was based on 11 MII oocytes. We used processed RNA-seq data of Fetal Primordial Germ Cells from Li et al (2017, Accession code: GSE86146) [PMID:28457750] from 17 human female embryos; and from Zhang et al (2018, Accession code GSE107746) [PMID: 30472193] ovarian tissue from 7 adult donors. For analysis of gene expression in mouse environmentally-induced low ovarian reserve models, gene expression was measured in 8 biologically independent animals from different litters in each group. For sChek1, Chek1 cKO, and Chek2 mice, experiments were performed in multiple mice and litters as detailed in the results. To test the natural breeding efficiency, cages were set with one or two adult (2-months or 12-month-old) control or females with a male of proven fertility. Litter sizes and dates of delivery were registered for all litters obtained during a period for up to one year.
Randomization	NA for population genetic analyses - all subjects with the available phenotype were included. For mouse environmentally-induced low ovarian reserve models, mice were randomized to different diets. There was no significant difference in the pre-culling litter size between obesogenic and control litters. Equal sex ratios within the litters were maintained as far as possible. For sChek1, Chek1 cKO, and Chek2 mice no randomization of the oocytes was performed as at each stage only the material necessary for the experiment was collected. All experiments were carried out using litter mate controls or with animals of closely related parents as controls.
Blinding	NA for genome-wide analyses - all subjects with the available phenotype were included. No blinding during data collection/analyses for mouse models. In the case of the environmentally-induced low ovarian reserve models, this was because mice were fed different diets. In the case of the Chek1, Chek1 cKO, and Chek2 models, this was as mice were genotyped two times, initially upon weaning and again before experimental procedures were carried out.

Reporting for specific materials, systems and methods

We require information from authors about some types of materials, experimental systems and methods used in many studies. Here, indicate whether each material, system or method listed is relevant to your study. If you are not sure if a list item applies to your research, read the appropriate section before selecting a response.

Materials & experimental systems

n/a	Involved in the study
☐	☒ Antibodies
☒	☐ Eukaryotic cell lines
☒	☐ Palaeontology and archaeology
☐	☒ Animals and other organisms
☐	☒ Human research participants
☒	☐ Clinical data
☒	☐ Dual use research of concern

Methods

n/a	Involved in the study
☒	☐ ChIP-seq
☒	☐ Flow cytometry
☒	☐ MRI-based neuroimaging

Antibodies

Antibodies used: Rhodamine (TRITC)-AffiniPure Donkey Anti-Rabbit IgG (711-025-152, Jackson Immuno Research)

Validation: As detailed on manufacturer's web site.

Animals and other organisms

Policy information about studies involving animals; ARRIVE guidelines recommended for reporting animal research

Laboratory animals: For mouse environmentally-induced low ovarian reserve model, female C57BL/6J mice were used. All animal experiments were carried out under the UK Home Office Animals (Scientific Procedures) Act (1986, United Kingdom). Female C57BL/6J mice were randomized to be fed ad libitum either a standard laboratory chow diet (7% simple sugars/3% fat; Special Dietary Services, Witham, UK) or an obesogenic diet.
sChek1, Chek1 cKO, and Chek2 mice: lines were maintained in a C57BL6 (Chek1cKO) or C57BL/6-129Sv (Chek2 and sChek1) mixed background, respectively. Breeding cages were set in a conventional way with strict specific pathogen-free barrier and mice used for experiments were kept in individual ventilated cages (IVC). 12h light exposure was provided. Temperature, relative humidity and air changes per hour were 22 °C (+/-2 °C), 55% +/-10 %, and 17 respectively. Food and water were provided ad libitum. Age of mice included in specific experiments is detailed in the results.

Wild animals: The study did not involve wild animals.

Field-collected samples: The study did not involve samples collected from the field.

Ethics oversight: For mouse environmentally-induced low ovarian reserve models: All animal experiments underwent ethical review by the University of Cambridge Animal Welfare and Ethical Review Board and were carried out under the UK Home Office Animals (Scientific Procedures) Act (1986, United Kingdom).
sChek1, Chek1 cKO, and Chek2 mice: Mouse work at the University of Copenhagen (sChek1) was licensed under 2016-15-0202-00043 by the Danish Animal Experiments Inspectorate (Dyreforsøgstilsynet, Denmark). Mouse work at UAB (Chek2) was approved by the UAB and the Catalan Ethics Committee for Animal Experimentation (CEEAAH 1091; DAAM6395). Mouse work at CCHMC (Chek1) was performed according to the guidelines of the Institutional Animal Care and Use Committee (protocol no. IACUC2018-0040) approved by CCHMC. The Chek1 cKO, Zp3-Cre embryology was conducted at the Institute of Animal Physiology and Genetics CAS in Libechov (Czech Republic), abiding by the policies of the Expert Committee for the Approval of Projects of Experiments on Animals of the Academy of Sciences of the Czech Republic (# 43-2015).

Note that full information on the approval of the study protocol must also be provided in the manuscript.

Human research participants

Policy information about studies involving human research participants

Population characteristics: For studies included in the genome-wide analyses, details of sample size, mean age and mean age at natural menopause for each study are provided in Supplementary Table 1. We included women with age at natural menopause (ANM) from age 40 to 60 inclusive. ANM was derived from self-reported questionnaire data by each study (details of questions are provided in Supplementary Table 1) and was the age at last naturally occurring menstrual period followed by at least 12 consecutive months of amenorrhea. Exclusions were women with menopause caused by hysterectomy, bilateral ovariectomy, radiation or chemotherapy, and those using HRT before menopause.

Recruitment: A range of study cohorts with data on post-menopausal European women were included in the genome-wide analyses - these included various study designs e.g. population cohort studies (e.g. UK Biobank), cancer studies (e.g. BCAC), and longitudinal studies (e.g. ALSPAC).

Ethics oversight

For studies included in the genome-wide analyses, within each of the studies, each participant provided written informed consent and the study protocol was approved by the institutional review board at the parent institution.
Research on RNA expression in human eggs was carried out according to the Helsinki II declaration and was conducted in accordance with national regulation on research on human subjects and material. The research was approved by the Scientific Ethical Committee of the Capital Region of Denmark (Videnskabsetisk Komite) in accordance with Danish National regulation (H-2-2011-044; extension license amm. Nr. 51307; license holder: Claus Yding Andersen and H-1604473; license holder: Eva R. Hoffmann; H-16027088 granted to Marie Louise Grøndahl). GDPR approval was obtained from the national data agency (SUND-2016-60, Eva R Hoffmann and HGH-2016_086 to Marie Louise Grøndahl).

Note that full information on the approval of the study protocol must also be provided in the manuscript.